Shell elements with through-the-thickness variable kinematics for the analysis of laminated composite and sandwich structures

Shell elements with through-the-thickness variable kinematics for the analysis of laminated composite and sandwich structures

E. Carrera, A. Pagani, S. Valvano

Department of Mechanical and Aerospace Engineering,
Politecnico di Torino, Turin, Italy

Keywords:
Variable kinematics, Equivalent single layer, Layer wise, Finite element method, Carrera unified formulation, Shells.

Author and address for Correspondence
Dr. Erasmo Carrera
Full Professor,
Department of Mechanical and Aerospace Engineering
Politecnico di Torino,
Corso Duca degli Abruzzi, 24,
10129 Torino, ITALY,
tel +39.011.546.6836, fax +39.011.564.6899
e.mail: erasmo.carrera@polito.it

Abstract

Several efforts have been made in the last years to improve the efficiency and the effectiveness of structural models for the analysis of laminated shell structures. Among the others, many recent and past works in the literature have been aimed at formulating theories of structures that maximize the accuracy of analysis meanwhile reducing the computational costs. In this paper, this objective is pursued by implementing advanced shell theories with through-the-thickness variable kinematic capabilities. By employing the Carrera Unified Formulation (CUF), the proposed shell model is obtained by expressing the displacement field as an arbitrary and, eventually, hierarchical expansion of the primary unknowns along the thickness. Thus, Equivalent-Single-Layer (ESL), Layer-Wise (LW) models as well as variable kinematic models which combine ESL and LW approaches within the shell thickness can be obtained in a straightforward and unified manner. After the unified shell model is formulated, the governing equations and the related finite element arrays are obtained by employing the principle of virtual work. A nine node finite element is implemented to approximate the solution field, and the Mixed Interpolation of Tensorial Components (MITC) method is used to contrast the membrane and shear locking phenomena. Some numerical examples are discussed, including three- and ten-layered cross-ply shells under bi-sinusoidal load and simply-supported boundary conditions, a multilayered spherical panel subjected to bi-sinusoidal load and a sandwich cylinder undergoing bi-sinusoidal pressure. Moreover, various thickness and radius-to-thickness ratios are considered. Whenever possible, the results are compared with those from the literature and from exact elasticity solutions. The analysis of the results clearly shows the enhanced capabilities of the present variable-kinematic shell element, which allows the analyst to opportunely reduce the computational costs and enhance the accuracy of the model only in those regions of the thickness domain where an accurate evaluation of the stress/strain field is needed.

1 Introduction

Nowadays, composite materials represent an important technology for Industry. In fact, composite layered plate and shell structures have a fundamental role in a variety of engineering applications, including aerospace and automotive design, among the others. Nevertheless, the analysis of the mechanical behavior of layered composite structures is not a simple issue in practice. Anisotropy, nonlinear analysis as well as complex phenomena, such as trough-the-thickness C_z^0 *requirements* (i.e., zig-zag effects in the displacements and interlaminar continuity for the stresses [1]), the couplings between in-plane and out-of-plane strains, are some of the issues to face. In most of the practical problems, the solution demands the applications of approximated computational methods. An overview of several computational techniques for the analysis of laminated structures can be read in the comprehensive review articles [2, 3, 4]. However, some significant contributions are mentioned in the following for the sake of completeness.

For the analysis of layered structures, the Finite Element Method (FEM) has a predominant role among the computational techniques used in the engineering practice. In the literature, the major part of FEM theories available is formulated on the basis of axiomatic-type theories. The most common used FEM element is the one based on classical Kirchhoff-Love theory and some examples are given in [5, 6]. Another classical plate/shell element is based on the First-order Shear Deformation Theory (FSDT), whose formulation can be found in the works by Pryor and Barker [7], Noor [8], Hughes [9] and many others.

A large variety of plate/shell finite element implementations of Higher-Order Theories (HOT) has been proposed in the last decades. HOT-based C^0 finite elements (C^0 means that the inter-element continuity is satisfied only for the unknown variables and not for their derivatives) were discussed by Kant and co-authors [10, 11]. Many other papers are available in which HOTs have been implemented for plates and shells, and more details can be found in the books by Reddy [12] and Palazotto and

Dennis [13]. In the domain of HOTs-based FEM elements, it is worth mentioning the zig-zag theories [14, 15, 16, 17], where the through-the-thickness solution concerning both displacements and stresses is enhanced by embedding discontinuous functions within the displacement field formulation.

Generally, for multilayered structures FEM analysis, two kinds of modeling approaches have been historically adopted in the literature. Namely, the Equivalent-Single-Layer (ESL) approach and the Layer-Wise (LW) approach. The HOT type theories mentioned above make use of the ESL approach, according to which the mechanical variables of the formulation (i.e., the unknowns) are independent of the number of layers. By contrast, the LW mathematical models allow considering different sets of variables per each layer. Finite element implementations of LW theories in the framework of axiomatic-type theories have been proposed by many authors, among which it is worth mentioning the works by Noor and Burton [18], Reddy [19], Mawenya and Davies [20], and Rammerstorfer *et al.* [21].

Although accurate, LW models may require the use of high computational efforts. Thus, in the last years, several efforts have been addressed by researchers to make the composite plate and shell models as accurate as efficient. A possible solution for tackling this problem is to combine multiple kinematics within the same mathematical model, in a global/local sense. In this manner, the computational costs can be reduced opportunely and the analysis enhanced only in those regions of the problem domain where accuracy is indispensable. One of the simple types of multiple-model method, for composite laminates analysis, is the concept of selective ply grouping or sublaminates [22, 23, 24]. This approach consists in creating some *local regions* along the plate/shell thickness, identified by specific ply or plies, within which accurate stresses are desired. On the other hand, in the global region, which is the domain portion where accurate analysis is not needed, lower-order and eventually ESL models can be adopted. Usually, in the literature, the local region is modeled by using 3-D finite elements for each ply, whereas the global region can be represented by 3-D finite elements grouped in one or more sublaminates. In the global region, the grouped sublaminates can be, hence, modeled with an ESL approach. The disadvantage of this approach is the use of the 3-D finite elements, which can be cumbersome and uncomfortable to handle from the pre-processing standpoint. Recently, the technique of selective ply grouping has been employed using only 2-D finite elements for both local and global regions in [25], where the authors of the present paper used a variable description in the thickness direction of the displacements for the implementation of global/local sublaminates plate elements.

The local region can be described more accurately by utilizing LW models, whereas the global region can be described by ESL models. Both ESL and LW models may eventually be implemented by using a combination of Lagrange and Legendre polynomials for formulating the theory kinematics along the thickness. In this manner, the primary variables between local and global regions can be immediately satisfied. In the work by Botshekanan Dehkordi *et al.* [26], a variable-kinematic description in the thickness direction for the static analysis of sandwich plates was performed. That model was derived in the framework of the Carrera Unified Formulation (CUF) and Reissner-Mixed-Variational-Theorem (RMVT) was adopted to describe apriori the transverse shear and normal stresses. Thus, the transverse stresses were approximated through a mixed LW/ESL approach. The same mixed LW/ESL approach with RMVT was then used in [27] for nonlinear dynamic analysis of sandwich plates with flexible core and composite faces embedded with shape memory alloy wires.

The global/local sublaminates approach based on mixed ESL/LW methodologies is, for the first time, extended to composite shell structures in this paper. The shell element makes use of the variable-kinematic modeling features of CUF, which was developed by Carrera more than one decade ago [28, 29] and allows for the automatic and eventually hierarchical formulation of the theory of structures by using an extensive index notation and low- to higher-order generalized expansions of the primary mechanical variables. Thanks to CUF, both ESL and LW theories can be formulated with ease and eventually combined as in the case of the present variable kinematics shell element. Also, the Mixed Interpolation of Tensorial Components (MITC) method [30, 31, 32, 33] is used in this work to contrast the membrane and shear lockings. The governing equations for the linear static analysis of composite

structures are derived from the principle of virtual work in a weak sense and the FEM is employed to obtain approximate numerical solutions for arbitrary geometries, laminations, and boundary conditions. In particular, cross-ply shells under bi-sinusoidal loads and simply-supported boundary conditions, a multilayered spherical panel subjected to bi-sinusoidal loads and a sandwich cylinder undergoing a bi-sinusoidal pressure and simply-supported boundary conditions are analyzed in this paper and compared with exact and approximate solutions from the literature.

The paper is organized as follows: First, (i) geometrical and constitutive relations for shells are presented in Section 2; Then, (ii) an overview of classical, higher-order and advanced shell theories developed within the CUF framework is given in Section 3; (iii) Section 4 gives a brief outline of the proposed FEM approach; Subsequently, (iv) the governing equations in weak form for the linear static analysis of composite structures are derived in Section 4.1; Next, (v) a short outline of the different modeling approaches is given, and the explanation of the present variable-kinematic sublaminates model is drawn in Section 5; Finally, (vi) the results obtained using the proposed CUF shell model are discussed and the main conclusions are drawn in Sections 6 and Section 7, respectively.

2 Geometrical and Constitutive relations

Shells are bi-dimensional structures in which one dimension (in general the thickness in the z direction) is negligible with respect to the other two dimensions. For the sake of completeness, the reference system of the shell is indicated in Fig. 1.

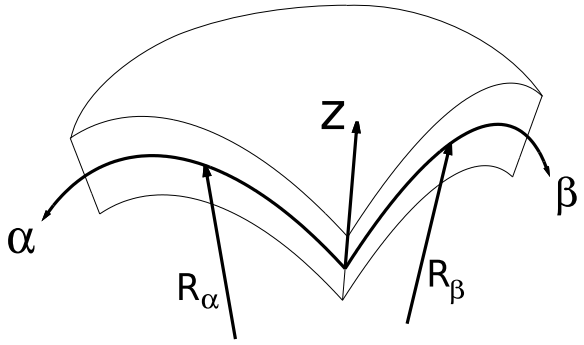

Figure 1: Reference system of the doubly-curved shell.

As far as multilayered structures are considered, the square of an infinitesimal linear segment in the layer, the associated infinitesimal area and volume are given as follows:

$$\begin{aligned} ds_k^2 = &\quad H_\alpha^{k\,2}\, d\alpha_k^2 \;+\; H_\beta^{k\,2}\, d\beta_k^2 + H_z^{k\,2}\, dz_k^2 \,, \\ d\Omega_k = &\quad H_\alpha^k H_\beta^k \, d\alpha_k \, d\beta_k \,, \\ dV = &\quad H_\alpha^k \, H_\beta^k \, H_z^k \, d\alpha_k \, d\beta_k \, dz_k \,, \end{aligned} \tag{1}$$

where the metric coefficients are

$$H_\alpha^k = A^k(1 + z_k/R_\alpha^k), \quad H_\beta^k = B^k(1 + z_k/R_\beta^k), \quad H_z^k = 1 \,. \tag{2}$$

k denotes the k-layer of the multilayered shell; R_α^k and R_β^k are the principal radii of the midsurface of the layer k. A^k and B^k are the coefficients of the first fundamental form of Ω_k (Γ_k is the Ω_k boundary). In this paper, the attention has been restricted to shells with constant radii of curvature (i.e., cylindrical,

spherical, toroidal geometries) for which $A^k = B^k = 1$. For further details on shells, interested readers can refer to the book by Reddy [12].

The geometrical relations enable to express the in-plane $\boldsymbol{\epsilon}_p^k$ and out-plane $\boldsymbol{\epsilon}_n^k$ strains in terms of the displacement $\boldsymbol{u}$ for each layer k. In the case of small displacements and rotations, one has:

$$\boldsymbol{\epsilon}_p^k = [\epsilon_{\alpha\alpha}^k, \epsilon_{\beta\beta}^k, \epsilon_{\alpha\beta}^k]^T = (\boldsymbol{D}_p^k + \boldsymbol{A}_p^k)\ \boldsymbol{u}^k\ ,\ \boldsymbol{\epsilon}_n^k = [\epsilon_{\alpha z}^k, \epsilon_{\beta z}^k, \epsilon_{zz}^k]^T = (\boldsymbol{D}_{n\Omega}^k + \boldsymbol{D}_{nz}^k - \boldsymbol{A}_n^k)\ \boldsymbol{u}^k\,. \tag{3}$$

The explicit forms of the arrays utilized in Eq. (3) are:

$$\boldsymbol{D}_p^k = \begin{bmatrix} \frac{\partial_\alpha}{H_\alpha^k} & 0 & 0 \\ 0 & \frac{\partial_\beta}{H_\beta^k} & 0 \\ \frac{\partial_\beta}{H_\beta^k} & \frac{\partial_\alpha}{H_\alpha^k} & 0 \end{bmatrix}, \quad \boldsymbol{D}_{n\Omega}^k = \begin{bmatrix} 0 & 0 & \frac{\partial_\alpha}{H_\alpha^k} \\ 0 & 0 & \frac{\partial_\beta}{H_\beta^k} \\ 0 & 0 & 0 \end{bmatrix}, \quad \boldsymbol{D}_{nz}^k = \begin{bmatrix} \partial_z & 0 & 0 \\ 0 & \partial_z & 0 \\ 0 & 0 & \partial_z \end{bmatrix}, \tag{4}$$

$$\boldsymbol{A}_p^k = \begin{bmatrix} 0 & 0 & \frac{1}{H_\alpha^k R_\alpha^k} \\ 0 & 0 & \frac{1}{H_\beta^k R_\beta^k} \\ 0 & 0 & 0 \end{bmatrix},\ \boldsymbol{A}_n^k = \begin{bmatrix} \frac{1}{H_\alpha^k R_\alpha^k} & 0 & 0 \\ 0 & \frac{1}{H_\beta^k R_\beta^k} & 0 \\ 0 & 0 & 0 \end{bmatrix}. \tag{5}$$

The linear stress-strain relations, as employed in this paper, are:

$$\begin{aligned} \boldsymbol{\sigma}_p^k &= \boldsymbol{C}_{pp}^k\ \boldsymbol{\epsilon}_p^k + \boldsymbol{C}_{pn}^k\ \boldsymbol{\epsilon}_n^k \\ \boldsymbol{\sigma}_n^k &= \boldsymbol{C}_{np}^k\ \boldsymbol{\epsilon}_p^k + \boldsymbol{C}_{nn}^k\ \boldsymbol{\epsilon}_n^k \end{aligned} \tag{6}$$

where

$$\begin{aligned} \boldsymbol{C}_{pp}^k &= \begin{bmatrix} C_{11}^k & C_{12}^k & C_{16}^k \\ C_{12}^k & C_{22}^k & C_{26}^k \\ C_{16}^k & C_{26}^k & C_{66}^k \end{bmatrix} \qquad \boldsymbol{C}_{pn}^k = \begin{bmatrix} 0 & 0 & C_{13}^k \\ 0 & 0 & C_{23}^k \\ 0 & 0 & C_{36}^k \end{bmatrix} \\ \boldsymbol{C}_{np}^k &= \begin{bmatrix} 0 & 0 & 0 \\ 0 & 0 & 0 \\ C_{13}^k & C_{23}^k & C_{36}^k \end{bmatrix} \qquad \boldsymbol{C}_{nn}^k = \begin{bmatrix} C_{55}^k & C_{45}^k & 0 \\ C_{45}^k & C_{44}^k & 0 \\ 0 & 0 & C_{33}^k \end{bmatrix} \end{aligned} \tag{7}$$

For the sake of brevity, the expressions that relate the material coefficients C_{ij} to the Young moduli E_1, E_2, E_3, the shear moduli G_{12}, G_{13}, G_{23} and Poisson ratios ν_{12}, ν_{13}, ν_{23}, ν_{21}, ν_{31}, ν_{32} are not given here. They can be found in [19].

3 Unified formulation of shells

Classical shell models grant good results when thin thickness, homogeneous structures are considered. On the other hand, the analysis of thick shells and multilayered structures may require more sophisticated theories to achieve sufficiently accurate solutions. As a general guideline, it is clear from a literature overview that the richer the kinematic terms in the shell displacement field, the more accurate the 2D model becomes. Carrera Unified Formulation (CUF) allows for the formulation of higher-order theories in which each displacement variable can be expanded up to any desired order in a hierarchical manner. Moreover, each primary variable can be treated independently from the others, according to the required accuracy. This procedure becomes extremely useful when multifield problems are investigated such as thermoelastic and piezoelectric applications [34, 35, 36, 37].

Generallyu, according to the CUF [29, 38, 39], the displacement field related to the k-th lamina of the shell structure can be written in the following unified manner:

$$\begin{aligned} u^k(\alpha,\beta,z) &= F_0(z)\, u_0^k(\alpha,\beta) + F_1(z)\, u_1^k(\alpha,\beta) + ... + F_N(z)\, u_N^k(\alpha,\beta) \\ v^k(\alpha,\beta,z) &= F_0(z)\, v_0^k(\alpha,\beta) + F_1(z)\, v_1^k(\alpha,\beta) + ... + F_N(z)\, v_N^k(\alpha,\beta) \\ w^k(\alpha,\beta,z) &= F_0(z)\, w_0^k(\alpha,\beta) + F_1(z)\, w_1^k(\alpha,\beta) + ... + F_N(z)\, w_N^k(\alpha,\beta) \end{aligned} \tag{8}$$

Or rather, in the compact form:

$$\boldsymbol{u}^k(\alpha,\beta,z) = F_s(z)\boldsymbol{u}_s^k(\alpha,\beta); \qquad \delta\boldsymbol{u}^k(\alpha,\beta,z) = F_\tau(z)\delta\boldsymbol{u}_\tau^k(\alpha,\beta) \qquad \tau,s = 0,1,...,N \tag{9}$$

where $\boldsymbol{u} = \{u, v, w\}$ is the displacement vector, whose components are expressed in the general reference system (α, β, z), see Fig. 1. $\delta\boldsymbol{u}$ is the virtual displacement vector associated to the virtual work and F_τ and F_s are the thickness functions depending only on z coordinate. τ and s are sum indexes and N is the number of terms of the expansion in the thickness direction assumed for the displacements. For the sake of clarity, the superscript k is omitted in the subsequent sections, where CUF models based on Taylor and Legendre F_τ/F_s polynomial expansions are addressed.

3.1 Taylor Higher-order Theories

Classical shell models that are usually utilized in the literature and in commercial finite element tools are based on Taylor expansions of the primary variables along the thickness direction. The Classical-Lamination-Theory (CLT) and the First-Shear-Deformation-Theory (FSDT), for example, are based on a Taylor polynomial expansion of the 3-D displacements including no more than constant and linear terms in z. As discussed in the introductory section, many attempts have been made to improve classical shell models. Refined theories, in general, make use of second- to higher-order polynomials for approximating the three-dimensional kinematic field along the shell thickness. Accordingly, CUF models based on Taylor polynomials express the unknown variables in terms of arbitrarily rich functions of the midplane position of the shell. This class of models are particularly efficient for thin and homogeneous structures.

In this paper, CUF Taylor-based higher-order shell models are expressed as

$$\boldsymbol{u} = F_0\, \boldsymbol{u}_0 + F_1\, \boldsymbol{u}_1 + \ldots + F_N\, \boldsymbol{u}_N = F_s\, \boldsymbol{u}_s, \qquad s = 0, 1, \ldots, N. \tag{10}$$

$$F_0 = z^0 = 1, \quad F_1 = z^1 = z, \quad \ldots, \quad F_N = z^N. \tag{11}$$

This class of models is denoted to as ETN, where E stands for Equivalent-Single-Layer (ESL, see Section 5), T stands for Taylor expansions, and N denotes the number of terms of the expansion and the polynomial order, which is arbitrary in the domain of CUF. For example, the $ET2$ model corresponds to a second-order shell model with the following kinematics:

$$\boldsymbol{u}(\alpha,\beta,z) = \boldsymbol{u}_0(\alpha,\beta) + z\, \boldsymbol{u}_1(\alpha,\beta) + z^2\, \boldsymbol{u}_2(\alpha,\beta) \tag{12}$$

Classical models, such as the CLT and FSDT, can be obtained as a particular case of an Equivalent-Single-Layer (ESL) theory with $N = 1$. Or, in other words, classical shell models are degenerated cases of the $ET1$ CUF model.

3.2 Legendre-like polynomial expansions

Expanding the unknown variables as functions of the shell midplane position can result in inaccurate results, especially when thick composite structures are addressed. A possible solution to this drawback

can be expanding the displacement field in *non-local* sense through-the-thickness by means, for example, of Legendre-like polynomials. These polynomial set, if formulated opportunely, can allow one to express the unknown variables in function of the top and bottom position of a given sub-domain of the shell thickness (i.e., each single layer or group of layers). In the case of Legendre-like polynomial expansion models, the displacement is defined as follows:

$$\boldsymbol{u} = F_0\,\boldsymbol{u}_0 + F_1\,\boldsymbol{u}_1 + F_r\,\boldsymbol{u}_r = F_s\,\boldsymbol{u}_s, \qquad s = 0, 1, r\ , \quad r = 2, ..., N. \tag{13}$$

$$F_0 = \frac{P_0 + P_1}{2}, \quad F_1 = \frac{P_0 - P_1}{2}, \quad F_r = P_r - P_{r-2}. \tag{14}$$

in which $P_j = P_j(\zeta)$ is the Legendre polynomial of j-order defined in the ζ-domain: $-1 \leq \zeta \leq 1$. $P_0 = 1$, $P_1 = \zeta$, $P_2 = (3\zeta^2 - 1)/2$, $P_3 = (5\zeta^3 - 3\zeta)/2$, $P_4 = (35\zeta^4 - 30\zeta^2 + 3)/8$.
For the Layer-Wise (LW) models, the Legendre polynomials and the relative top and bottom position are defined for each layer.

3.3 Refined polynomials with Zig-Zag Function

Due to the intrinsic anisotropy of multilayered structures, the first derivative of the displacement variables in the z-direction is discontinuous. It is possible to reproduce the zig-zag effect in the framework of the ESL description by employing the Murakami theory. According to [14], a zig-zag term can be introduced into Eq. (10) as follows:

$$\boldsymbol{u} = F_0(z)\,\boldsymbol{u}_0 + \ldots + F_{N-1}(z)\,\boldsymbol{u}_{N-1} + (-1)^k \zeta_k \boldsymbol{u}_N^k. \tag{15}$$

Equivalently, the zig-zag function can be introduce also into Eq. (13) for a further enhancement of the LW model:

$$\begin{aligned} &\boldsymbol{u} = F_0\,\boldsymbol{u}_0 + F_1\,\boldsymbol{u}_1 + F_r\,\boldsymbol{u}_r + (-1)^k \zeta_k \boldsymbol{u}_N^k. \\ &0 = \text{top}, \quad 1 = \text{bottom}, \qquad r = 2, ..., N-1 \end{aligned} \tag{16}$$

The models outlined in Eqs. (15) and (16) are called zig-zag theories. The zig-zag function is defined in each layer k, where the non-dimensional term ζ_k takes value 1 and -1 at the top and the bottom of each layer, respectively.

4 Finite Element approximation

Independently of the choice of the shell model kinematics, the Finite Element Model (FEM) can be employed for approximating the solution field within the structure midplane domain. According to FEM, the generalized displacements can be expressed as a linear combinations of the shape functions. Considering a 9-node finite element, the generalized displacement vector and the related variation are defined as follows:

$$\boldsymbol{u}_s(\alpha, \beta) = N_j(\alpha, \beta)\boldsymbol{u}_{s_j} \qquad \delta\boldsymbol{u}_\tau(\alpha, \beta) = N_i(\alpha, \beta)\delta\boldsymbol{u}_{\tau_i} \qquad \text{with} \quad i, j = 1, ..., 9 \tag{17}$$

where $\boldsymbol{u}_{s_j}$ and $\delta\boldsymbol{u}_{\tau_i}$ are the nodal displacements and their virtual variations, i and j denote summation, and N_i and N_j are the Lagrangian shape functions defined in the shell element domain. Substituting the FEM approximation (Eq. (17)) into the generalized displacement expansion (Eq. (9)), one has:

$$\begin{aligned} \boldsymbol{u}(\alpha, \beta, z) &= F_s(z) N_j(\alpha, \beta)\boldsymbol{u}_{s_j} \qquad s = 0, 1, ..., N \\ \delta\boldsymbol{u}(\alpha, \beta, z) &= F_\tau(z) N_i(\alpha, \beta)\delta\boldsymbol{u}_{\tau_i} \qquad \tau = 0, 1, ..., N \end{aligned} \tag{18}$$

As well known from previous literature, FEM can be affected by severe locking phenomena. Many solutions are available to overcome those numerical problems; e.g. reduced integration, selective integration [40], and the mixed interpolation of tensorial components (MITC) [30]. In this paper, a MITC technique is used to overcome the shear locking phenomenon. However, for the sake of brevity, details about the use of MITC in the domain of CUF are not discussed here, but further discussion can be found in Cinefra *et al.* [37].

4.1 Governing equations and related FE arrays

According to the principle of virtual work, the virtual variation of the internal strain energy of an equilibrated system is equivalent to the virtual variation of the external loadings; i.e.

$$\int_{\Omega_k}\int_{A_k} \left(\delta {\boldsymbol{\epsilon}_p^k}^T \boldsymbol{\sigma}_p^k + \delta {\boldsymbol{\epsilon}_n^k}^T \boldsymbol{\sigma}_n^k \right) \, d\Omega_k dz = \delta L_e \tag{19}$$

where Ω_k and A_k are the integration domains in the plane and the thickness direction, respectively. The left-hand side of the equation represents the variation of the internal work, while the right-hand side is the virtual variation of the external work. Substituting the constitutive equations (Eq. 6), the linear geometrical relations (Eq. 3) and applying CUF and the FEM approximation (Eq. 18) into Eq. (19), the governing equations can be obtained straightforwardly. In a compact form, the following system of linear algebraic equations holds:

$$\delta \boldsymbol{u}_{\tau_i}^k : \quad \boldsymbol{K}^{k\tau sij} \boldsymbol{u}_{sj}^k = \quad \boldsymbol{P}^{k\tau i} \tag{20}$$

where $\boldsymbol{K}^{k\tau sij}$ is a 3×3 matrix, called fundamental nucleus of the mechanical stiffness matrix, and its explicit expression is given in [41]. The nucleus is the basic element from which the stiffness matrix of the whole structure can be computed automatically. First, the fundamental nucleus is expanded on the indexes τ and s to obtain the stiffness matrix of each layer k. Then, the matrices of each layer are assembled at the multi-layer level depending on the approach considered (see Section 5). $\boldsymbol{P}^{k\tau i}$ is a 3×1 matrix, called fundamental nucleus of the external load.

The explicit expressions of the CUF fundamental nuclei for shell structures are not reported here. Complete formulation and related mathematical passages can be found in the recent book by Carrera *et al.* [42]. In this paper, the main attention is focused on the use of these hierarchical nuclei for the formulation of variable kinematics models with combined ESL and LW capabilities through the thickness of the shell, for the formulation of global/local theories.

5 Modelling Approaches

Two different types of modelling approaches are usually adopted in the literature for the formulation of composite structure theories; i.e., ESL and LW. In this paper, CUF formulation is employed for the formulation of a new approach for multilayered shells. This approach exploits the variable kinematics characteristics of CUF for the implementation of a shell element with mixed ESL/LW capabilities. Nevertheless, it is important to mention that choice of the modelling approach (i.e., ESL, LW or variable kinematics) is independent of the type of the polynomials employed in the theory expansion within CUF formulation.

5.1 ESL models

In an ESL model, the stiffness matrices of each layer are homogenized by simply summing the various contributions trough the thickness. This approach leads to a model that has a set of variables that is assumed for the whole multilayer, and thus is independent of the number of layers. In this work, ESL

models that make use of both Taylor and Legendre-like polynomials are used. For illustrative purposes, the general behaviour of the primary mechanical variables along the thickness of the structure in the case of ESL is depicted in Fig. 2.

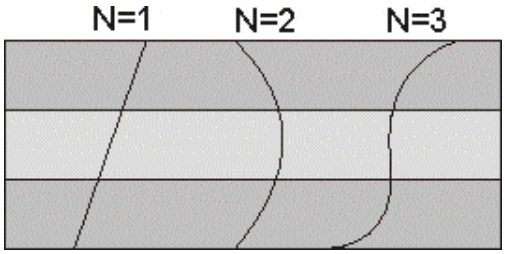

Figure 2: Equivalent-Single-Layer behaviour of the primary variables along the thickness of the shell.

5.2 LW models

In the case of LW, different sets of variables are assumed per each layer and the continuity of the displacements is imposed at the layer interface. The LW capability of describing correctly the discontinuous behaviour of the derivatives of the primary unknowns is graphically shown in in Fig. 3.

In this work, LW models are implemented by using Legendre-like polynomial sets. In particular, the kinematic expansion is made by using Lagrange and Legendre polynomials, see Eq. (13). The Lagrange polynomials F_0 and F_1, in fact, are necessary for interpolating the displacements at the top (t) and bottom (b) position of the layer, respectively. Hence, the unknown variables at the top (t) and bottom (b) position are used to impose the following compatibility conditions:

$$\boldsymbol{u}_t^k = \boldsymbol{u}_b^{k+1}, \qquad k = 1, N_l - 1. \tag{21}$$

where N_l is the number of layers.

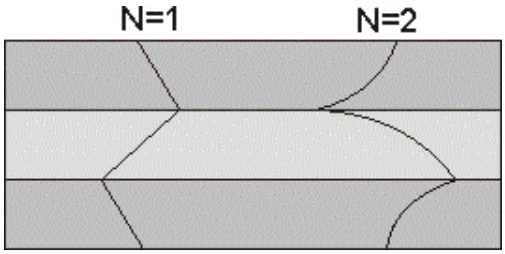

Figure 3: Layer-Wise behaviour of the primary variables along the thickness of the shell.

5.3 Variable-Kinematics

In this paper, a novel modelling approach for the analysis of multilayered shells is introduced. This method takes advantage of the variable kinematics feature of CUF formulation. Thanks to CUF, in fact, different sets of F_τ and F_s thickness functions can be employed to formulate advanced structural theories and opportunely tuned for resulting into combined ESL/LW models for global/local analysis. In particular, in this work, ESL and LW approaches are combined by employing structural theories based on Legendre-like polynomials. In this variable-kinematics approach, multilayered structures

can be modelled so as to have group of layers with homogenized properties as in a ESL assembling scheme, whereas for some other layers the homogenization is conducted just at the interface level for enforcing LW capabilities in localized zones of the thickness domain. The variable-kinematic assembling, developed in the framework of the CUF, is very simple to integrate with a few code statements. The coding lines of the terms of the nuclei, in fact, are the same for both ESL, LW and variable kinematic assembling.

For the sake of completeness, the variable kinematic capability of the proposed methodology to take into account for non-local LW approach is shown in Fig. 4. Moreover, an overview of the assembling procedures for ESL, LW and variable kinematics approaches is summarized in Fig. 5.

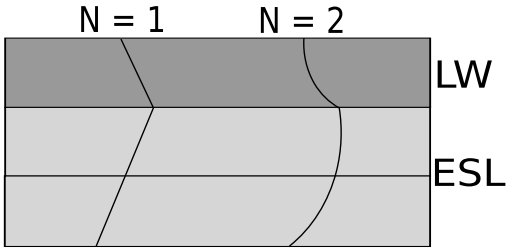

Figure 4: Variable-kinematics model behaviour of the primary variables along the thickness of the shell.

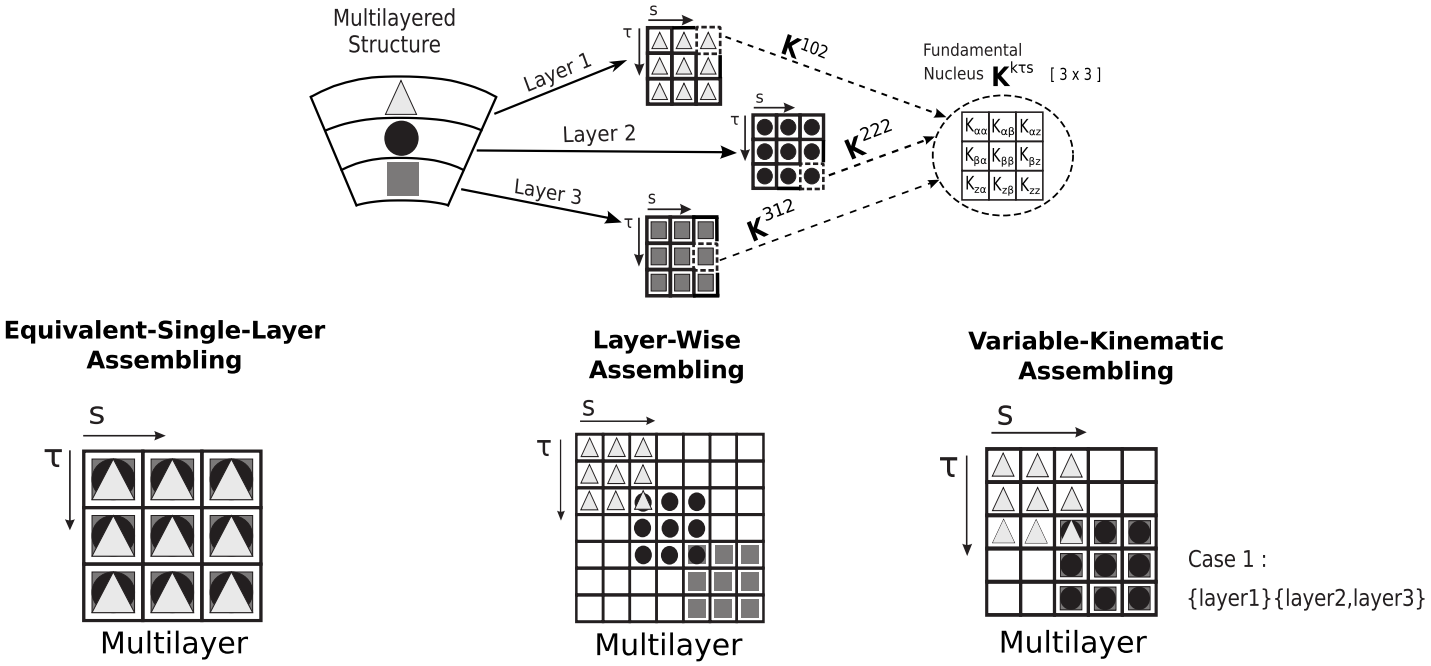

Figure 5: Overview of assembling schemes for ESL, LW and variable kinematics approaches.

Acronyms

Depending on the variables description, the modelling approach and the number of terms N of the kinematic expansion, different shell theories can be obtained. For the sake of clearness, a system of acronyms is given in order to denote these models. The first letters in the acronym indicate the approach used, i.e. equivalent single layer (E) or layer-wise (LW). In the case of ESL models, the second letter

denotes the type of polynomial adopted: (T) for the Taylor polynomial expansions or (L) for the the Legendre-like polynomials. The number N at the end of the acronym indicates the number of terms of the expansion used in the thickness direction. Eventually, a Z is added to denote the zig-zag terms into the kinematic expansion, whereas the subscript (a) indicates that analytical solution is provided instead of FEM. On the other hand, variable kinematic models are discussed below depending on each case.

6 Numerical results

The following reference problems have been considered for assessing the novel variable kinematic shell element:

- A three-layer simply-supported cylinder with $(90°/0°/90°)$ lamination.
- A ten-layer simply-supported cylinder with $(90°/0°/90°/0°/90°)_S$ lamination.
- A composite square simply-supported spherical panel with three-layer configuration $(0°/90°/0°)$ and four-layer configuration $(0°/90°/90°/0°)$.
- An eleven-layer simply-supported sandwich cylindrical panel with $(0°/90°/0°/Core/0°/\ 90°/0°/Core/0°/90°/0°)$ lamination.

Wherever possible, solutions from variable-kinematic models are compared with those from higher-order ESL models, LW models, 3D elasticity solutions and analytical results.

6.1 Three-layer composite cylinder

A three-layer cross-ply cylinder with lamination $(90°/0°/90°)$ and simply-supported boundary conditions is considered as the first numerical example. The applied load for the whole cylinder is a pressure applied at the inner surface of the shell, defined as follows:

$$p\left(\alpha,\beta,z_{bottom}\right)=\hat{p}\,sin\left(\frac{m\pi\alpha}{a}\right)cos\left(\frac{n\pi\beta}{b}\right) \tag{22}$$

where $\hat{p}=1.0$ is the pressure amplitude; $m=1$ and $n=8$; α and β are the coordinates as defined in Fig. 1; and a and b are the shell dimensions along α and β, respectively. Note that a is the length of the cylinder in the axial direction in this example. The mechanical properties of the material are such that $E_L/E_T=25$; $G_{LT}/E_T=0.5$; $G_{TT}/E_T=0.2$; $\nu_{LT}=\nu_{TT}=0.25$. For all the considered cases, the length-to-radius ratio is $a/R=4$, $b=2\pi R$. On the other hand, the layers are of equal thickness and $h_{total}=1,0$. The results are presented below for different radius-to-thickness ratios $R/h=2,4,10,50,100,500$, and reported in the following non-dimensional form:

$$\hat{w}=\frac{10wE_L}{\hat{p}h(R/h)^4}\qquad \hat{\sigma}_{\alpha\alpha/\beta\beta/\alpha\beta}=\frac{10\sigma_{\alpha\alpha/\beta\beta/\alpha\beta}}{\hat{p}(R/h)^2}\qquad \hat{\sigma}_{\alpha z/\beta z}=\frac{10\sigma_{\alpha z/\beta z}}{\hat{p}(R/h)}\qquad \hat{\sigma}_{zz}=\frac{\sigma_{zz}}{\hat{p}}$$

Due to the geometrical symmetry of the cylinder, the symmetry of the load pressure and boundary conditions, and the symmetry of the lamination stacking sequence, only one octave of the cylinder is analysed; i.e., only one half of the cylinder along the α axis direction and one quarter along the β circumferential axis direction is considered. The applied load for an octave of the cylinder is, therefore, defined as follows:

$$p\left(\alpha,\beta,z_{bottom}\right)=\hat{p}\,cos\left(\frac{m\pi\alpha}{a}\right)cos\left(\frac{n\pi\beta}{b}\right) \tag{23}$$

where $m = 0, 5$ and $n = 2$. The FEM results coming from the present refined CUF shell elements are compared with a 3D elasticity solution [43] and a layer-wise analytical model [39].

First, a convergence study on the shell element was performed. A representative composite shell with radius-to-thickness ratio $R/h = 500$ was evaluated. According to Table 1, a mesh grid of 8×32 elements ensures the convergence and accuracy on both the transverse displacement and the stresses. Thus, this mesh size is used in the subsequent analyses. Furthermore, in order to prove that the proposed element is locking free, various integrations schemes (see Huges *et al.* [40]) were considered and the results are shown in Table 2. In this table, the results from the present higher-order finite elements are compared to 3D analytical solutions. It is clear that the shell element with the MITC9 method ensures acceptable accuracy on both the transverse displacement, the transverse shear stress and the transverse normal stress. In both Tables 1 and 2, superscript + denotes that stress is measured at the layer interface and the top value is given.

Table 1: Convergence study. Composite cylinder with lamination $[90°/0°/90°]$ and with radius to thickness ratio $R/h = 500$. The mesh is referred to one octave of the cylinder.

	Mesh	2×8	4×16	6×24	8×32	*3D Elasticity* [43]
$LW4$	$\hat{w}\ (z = 0)$	0.1029	0.1027	0.1027	0.1027	0.1027
	$\hat{\sigma}_{\alpha\alpha}\ (z = +h/2)$	0.0586	0.0566	0.0562	0.0560	0.0559
	$\hat{\sigma}_{\beta\beta}\ (z = +h/2)$	0.8279	0.7994	0.7940	0.7921	0.7895
	$\hat{\sigma}_{\alpha z}\ (z^+ = -h/6)$	0.1107	0.1066	0.1058	0.1055	0.1051
	$\hat{\sigma}_{zz}\ (z = 0)$	-7.15	-9.04	-9.13	-9.13	-9.12
$ET4$	$\hat{w}\ (z = 0)$	0.1029	0.1027	0.1027	0.1027	
	$\hat{\sigma}_{\alpha\alpha}\ (z = +h/2)$	0.0589	0.0568	0.0564	0.0563	
	$\hat{\sigma}_{\beta\beta}\ (z = +h/2)$	0.8283	0.7998	0.7944	0.7925	
	$\hat{\sigma}_{\alpha z}\ (z^+ = -h/6)$	0.1400	0.1348	0.1338	0.1334	
	$\hat{\sigma}_{zz}\ (z = 0)$	15.41	12.84	12.61	12.56	
$EL4$	$\hat{w}\ (z = 0)$	0.1029	0.1027	0.1027	0.1027	
	$\hat{\sigma}_{\alpha\alpha}\ (z = +h/2)$	0.0589	0.0568	0.0564	0.0563	
	$\hat{\sigma}_{\beta\beta}\ (z = +h/2)$	0.8283	0.7998	0.7944	0.7925	
	$\hat{\sigma}_{\alpha z}\ (z^+ = -h/6)$	0.1400	0.1348	0.1338	0.1334	
	$\hat{\sigma}_{zz}\ (z = 0)$	15.41	12.84	12.61	12.56	

Table 2: Locking study. Composite cylinder with lamination [90°/0°/90°] and with radius to thickness ratio $R/h = 500$. All the present FEM analyses are computed with a mesh of 8×32 elements.

		Reduced	*Selective*	$MITC9$	*Analytical*
$3D$ *Elasticity* [43]	$w\ (z=0)$				0.1027
	$\sigma_{\alpha z}\ (z^+=-h/6)$				0.1051
	$\sigma_{zz}\ (z=0)$				-9.12
$LW4$	$w\ (z=0)$	0.1027	0.1023	0.1027	
	$\sigma_{\alpha z}\ (z^+=-h/6)$	1.2767	0.1070	0.1055	
	$\sigma_{zz}\ (z=0)$	-52.14	-9.70	-9.13	
$EL4$	$w\ (z=0)$	0.1027	0.1023	0.1027	
	$\sigma_{\alpha z}\ (z^+=-h/6)$	1.3152	0.1368	0.1334	
	$\sigma_{zz}\ (z=0)$	-30.52	15.00	12.56	
$ET4$	$w\ (z=0)$	0.1027	0.1023	0.1027	
	$\sigma_{\alpha z}\ (z^+=-h/6)$	1.3152	0.1368	0.1334	
	$\sigma_{zz}\ (z=0)$	-30.52	15.00	12.56	

An assessment of the Legendre-like and Taylor based ESL models is performed next. All the results presented in Table 3, for thick and thin shells, show that the Legendre polynomials lead to the same results of the Taylor polynomials. Regarding the linear expansion ESL model, e.g. $ET1$, if the thickness locking correction is applied (see [42]), a moderate difference in the results is noticeable. Nevertheless, the use of either polynomials is invariant with respect to the solution accuracy, thus, Legendre-like models are indistinctly used to implement ESL, LW as well as variable-kinematic models in the analyses below.

Table 3: Composite three-layered cylinder with lamination [90°/0°/90°]. Taylor vs Legendre models.

		$\hat{w}$	$\hat{\sigma}_{\alpha\alpha}$		$\hat{\sigma}_{\beta\beta}$		$\hat{\sigma}_{\alpha\beta}$		$\hat{\sigma}_{\alpha z}$	$\hat{\sigma}_{\beta z}$	$\hat{\sigma}_{zz}$	$DOFs$
	$z =$	0	$+h/2$	$-h/2$	$+h/2$	$-h/2$	$+h/2$	$-h/2$	$-h/6$	0	0	
$R/h = 500$	$3D\ Elasticity$[43]	0.1027	0.0559	0.0379	0.7895	-0.7542	-0.0766	-0.0889	0.1051	-0.691	-9.12	
	$LW4$	0.1027	0.0560	0.0380	0.7921	-0.7567	-0.0771	-0.0894	0.1055	-0.693	-9.13	43095
	$EL3Z$	0.1027	0.0561	0.0380	0.7921	-0.7567	-0.0771	-0.0894	0.0586	-0.703	-9.47	16575
	$EL4$	0.1027	0.0563	0.0383	0.7925	-0.7563	-0.0771	-0.0894	0.1334	-0.494	12.56	16575
	$EL3$	0.1027	0.0564	0.0383	0.7925	-0.7563	-0.0771	-0.0894	0.0615	-0.494	12.56	13260
	$EL2$	0.1027	0.0557	0.0377	0.7918	-0.7571	-0.0771	-0.0894	0.0611	-0.250	43.39	9945
	$EL1$	0.1026	0.0584	0.0349	0.7945	-0.7597	-0.0770	-0.0894	0.0106	-0.250	43.23	6630
	$ET3Z$	0.1027	0.0561	0.0380	0.7921	-0.7567	-0.0771	-0.0894	0.0586	-0.703	-9.47	16575
	$ET4$	0.1027	0.0563	0.0383	0.7925	-0.7563	-0.0771	-0.0894	0.1334	-0.494	12.56	16575
	$ET3$	0.1027	0.0564	0.0383	0.7925	-0.7563	-0.0771	-0.0894	0.0615	-0.494	12.56	13260
	$ET2$	0.1027	0.0557	0.0377	0.7918	-0.7571	-0.0771	-0.0894	0.0611	-0.250	43.39	9945
	$ET1^{-}$	0.1026	0.0584	0.0349	0.7945	-0.7597	-0.0770	-0.0894	0.0106	-0.250	43.23	6630
	$ET1^{*}$	0.1032	0.0529	0.0348	0.7971	-0.7585	-0.0770	-0.0894	0.0100	-0.250	43.42	6630
$R/h = 2$	$3D\ Elasticity$[43]	10.11	0.1761	-0.8428	7.168	-18.19	0.1797	-0.2922	0.3006	-1.379	-0.34	
	$LW4$	10.10	0.1741	-0.8730	7.179	-18.17	0.1807	-0.2934	0.3018	-1.382	-0.34	43095
	$EL3Z$	9.65	0.1487	-0.8951	6.848	-14.15	0.1728	-0.2653	0.2679	-1.294	-0.32	16575
	$EL4$	9.59	0.1425	-0.9572	6.568	-15.63	0.1775	-0.2783	0.4244	-1.219	-0.35	16575
	$EL3$	9.54	0.1431	-0.9179	7.048	-14.65	0.1785	-0.2706	0.3704	-1.216	-0.35	13260
	$EL2$	8.16	0.0965	-0.6479	0.981	-5.88	0.1208	-0.2025	0.3183	-0.847	-0.43	9945
	$EL1$	8.82	-0.1046	-0.3218	2.441	-3.79	0.1542	-0.2152	0.2941	-0.927	-0.37	6630
	$ET3Z$	9.65	0.1487	-0.8951	6.848	-14.15	0.1728	-0.2653	0.2679	-1.294	-0.32	16575
	$ET4$	9.59	0.1425	-0.9572	6.568	-15.63	0.1775	-0.2783	0.4244	-1.219	-0.35	16575
	$ET3$	9.54	0.1431	-0.9179	7.048	-14.65	0.1785	-0.2706	0.3704	-1.216	-0.35	13260
	$ET2$	8.16	0.0965	-0.6479	0.981	-5.88	0.1208	-0.2025	0.3183	-0.847	-0.43	9945
	$ET1^{-}$	8.82	-0.1046	-0.3218	2.441	-3.79	0.1542	-0.2152	0.2941	-0.927	-0.37	6630
	$ET1^{*}$	8.83	-0.1193	-0.3081	2.442	-3.79	0.1556	-0.2160	0.2922	-0.927	-0.37	6630

$*$ *thickness locking correction*
$-$ *no correction*

Different variable kinematic models are used to perform the global/local analysis of the cylindrical shell structures and they are graphically depicted in Fig. 6. Two different sublaminate groupings are considered here and they are denoted to as:

- $Case\,1 = \{layer1\}\,\{layer2, layer3\}$
- $Case\,2 = \{layer1, layer2\}\,\{layer3\}$

In $Case\,1$, for example, layers number 2 and 3 are grouped in an ESL manner and then assembled to layer 1 in a LW sense, see Fig. 6. $Case\,1$ and $Case\,2$ are used as subscripts together with the usual acronym notation, which also indicates the theory order N.

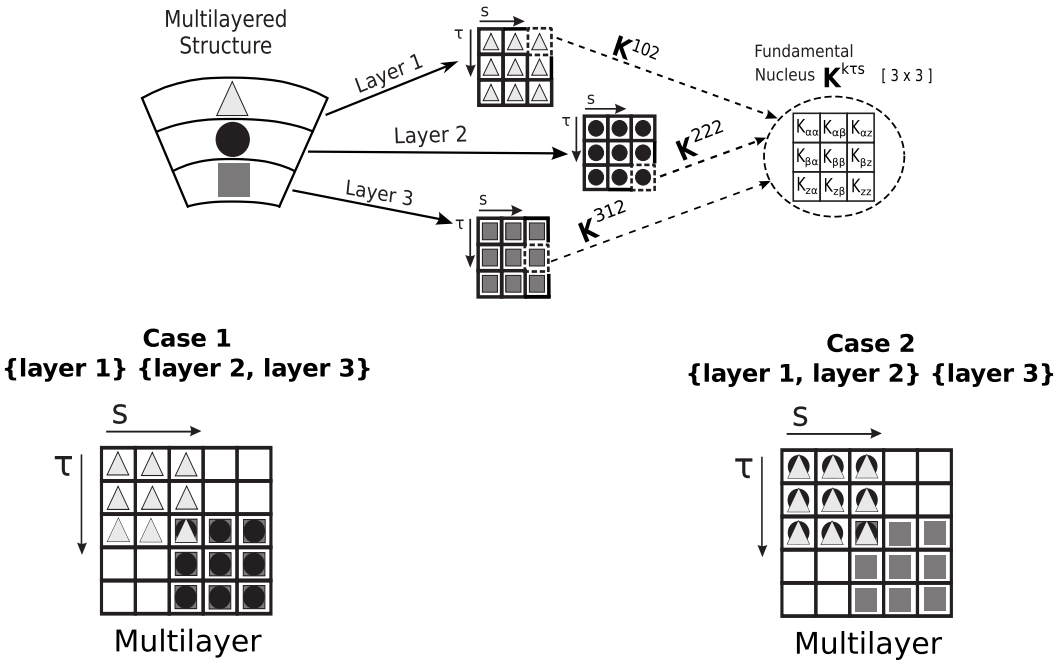

Figure 6: Variable-kinematic assembly schemes for the three-layered cylindrical shell.

The results from present variable kinematic models are listed in Tables 4 and 5 and Figs 7 to 14 for various radius to thickness ratios R/h. For the shell structures analysed, the following considerations can be drawn:

- Regarding the transverse displacement w, the theories $EL4_{,Case\,1}$ and $EL4_{,Case\,2}$ lead a significant improvement of the solution with respect to $EL4$ for large radius-to-thickness ratios $R/h = 500$, see Fig. 7. On the other hand, if small ratios $R/h = 2$ are considered, differences among the various models adopted are barely observable from Fig. 8.

- For the in-plane stress $\sigma_{\beta\beta}$, no accuracy differences are appreciable between models for ratios $R/h = 500$, see Fig. 9. For small ratios $R/h = 2$ the theories $EL4_{,Case\,1}$ and $EL4_{,Case\,2}$ improve the results with respect to the $EL4$ model, especially where a layer-wise description within the variable-kinematics is adopted; i.e., the top layer for $EL4_{,Case\,1}$ and the bottom layer for $EL4_{,Case\,2}$, see Fig. 10.

- As far as the shear stress $\sigma_{\alpha z}$ is concerned, Figs. 11 and 12 show that the variable kinematic models provide exact solution accuracy for every radius-to-thickness-ratios within the layers that have a layer-wise assembling. Conversely, the remaining layers with an equivalent-single-layer assembling have a loss of accuracy.

- Regarding the transverse normal stress σ_{zz} and for large ratios $R/h = 500$, the results reach the exact solution in the layers that have a layer-wise assembling and a variable kinematic approach, see Fig. 13. Instead, for small ratios $R/h = 2$ the theories $EL4_{,Case\,2}$ approximate very well the layer-wise solution along the thickness, see Fig. 14.

- For all the considered cases, the variable kinematic models have a number of degrees of freedom, and thus a computational cost, which is lower that full LW models.

Table 4: Composite three-layered cylinder with [90°/0°/90°] lamination. Comparison of various models for thin cylinders.

		$\hat{w}$	$\hat{\sigma}_{\alpha\alpha}$		$\hat{\sigma}_{\beta\beta}$		$\hat{\sigma}_{\alpha\beta}$		$\hat{\sigma}_{\alpha z}$	$\hat{\sigma}_{\beta z}$	$\hat{\sigma}_{zz}$	$DOFs$
	$z =$	0	$+h/2$	$-h/2$	$+h/2$	$-h/2$	$+h/2$	$-h/2$	$-h/6$	0	0	
$R/h = 500$	$3D\ Elasticity$[43]	0.1027	0.0559	0.0379	0.7895	-0.7542	-0.0766	-0.0889	0.1051	-0.691	-9.12	
	$LW4$	0.1027	0.0560	0.0380	0.7921	-0.7567	-0.0771	-0.0894	0.1055	-0.693	-9.13	43095
	$LW1$	0.1027	0.0569	0.0370	0.7931	-0.7578	-0.0771	-0.0894	0.0092	-0.692	-9.12	13260
	$EL3Z$	0.1027	0.0561	0.0380	0.7921	-0.7567	-0.0771	-0.0894	0.0586	-0.703	-9.47	16575
	$EL4$	0.1027	0.0563	0.0383	0.7925	-0.7563	-0.0771	-0.0894	0.1334	-0.494	12.56	16575
	$EL1$	0.1026	0.0584	0.0349	0.7945	-0.7597	-0.0770	-0.0894	0.0106	-0.250	43.23	6630
	$EL4_{Case\,1}$	0.1027	0.0560	0.0379	0.7921	-0.7569	-0.0771	-0.0894	0.1323	-0.698	-16.56	29835
	$EL1_{Case\,1}$	0.1027	0.0569	0.0357	0.7930	-0.7590	-0.0771	-0.0894	0.0445	-0.311	119.23	9945
	$EL4_{Case\,2}$	0.1027	0.0559	0.0380	0.7919	-0.7567	-0.0771	-0.0894	0.0965	-0.699	-11.98	29835
	$EL1_{Case\,2}$	0.1027	0.0574	0.0370	0.7936	-0.7579	-0.0771	-0.0894	-0.0244	-0.316	-58.85	9945
$R/h = 100$	$3D\ Elasticity$[43]	0.4715	0.0838	0.0018	3.507	-3.507	-0.0478	-0.1038	0.1223	-3.127	-8.30	
	$LW2_a$[39]	0.4715	-	-	-	-	-	-	-	-3.127	-8.29	
	$ESL2_a$[39]	0.4694	-	-	-	-	-	-	-	-	-	
	$LW4$	0.4715	0.0841	0.0018	3.518	-3.518	-0.0481	-0.1045	0.1228	-3.137	-8.32	43095
	$LW1$	0.4711	0.0869	-0.0034	3.518	-3.520	-0.0481	-0.1044	0.0385	-3.131	-8.31	13260
	$EL3Z$	0.4715	0.0842	0.0017	3.518	-3.518	-0.0481	-0.1045	0.0781	-3.183	-8.63	16575
	$EL4$	0.4708	0.0841	0.0021	3.517	-3.517	-0.0480	-0.1043	0.1576	-2.237	-8.00	16575
	$EL1$	0.4674	0.0939	-0.0121	3.512	-3.512	-0.0477	-0.1036	0.0450	-1.131	-4.32	6630
	$EL4_{Case\,1}$	0.4714	0.0841	0.0017	3.518	-3.518	-0.0481	-0.1044	0.1627	-3.161	-9.06	29835
	$EL1_{Case\,1}$	0.4688	0.0866	-0.0083	3.513	-3.514	-0.0478	-0.1039	0.0732	-1.416	10.77	9945
	$EL4_{Case\,2}$	0.4714	0.0841	0.0018	3.518	-3.517	-0.0481	-0.1044	0.1223	-3.160	-8.23	29835
	$EL1_{Case\,2}$	0.4691	0.0898	-0.0035	3.513	-3.517	-0.0478	-0.1040	0.0120	-1.424	-21.35	9945
$R/h = 50$	$3D\ Elasticity$[43]	0.5495	0.0712	-0.0225	3.930	-3.987	-0.0118	-0.0760	0.0894	-3.491	-4.85	
	$LW2_a$[39]	0.5495	-	-	-	-	-	-	-	-3.492	-4.73	
	$ESL2_a$[39]	0.5384	-	-	-	-	-	-	-	-	-	
	$LW4$	0.5495	0.0715	-0.0225	3.943	-3.999	-0.0119	-0.0765	0.0897	-3.502	-4.86	43095
	$LW1$	0.5479	0.0732	-0.0297	3.933	-3.995	-0.0118	-0.0763	0.0439	-3.497	-4.85	13260
	$EL3Z$	0.5495	0.0718	-0.0229	3.943	-4.000	-0.0119	-0.0765	0.0626	-3.554	-5.03	16575
	$EL4$	0.5458	0.0711	-0.0225	3.937	-3.993	-0.0117	-0.0761	0.1161	-2.501	-5.02	16575
	$EL1$	0.5358	0.0799	-0.0390	3.900	-3.957	-0.0115	-0.0748	0.0508	-1.265	-3.39	6630
	$EL4_{Case\,1}$	0.5487	0.0714	-0.0225	3.941	-3.998	-0.0119	-0.0764	0.1237	-3.529	-5.07	29835
	$EL1_{Case\,1}$	0.5385	0.0724	-0.0348	3.916	-3.954	-0.0115	-0.0751	0.0650	-1.582	0.69	9945
	$EL4_{Case\,2}$	0.5488	0.0715	-0.0225	3.942	-3.998	-0.0118	-0.0764	0.0949	-3.527	-4.84	29835
	$EL1_{Case\,2}$	0.5391	0.0752	-0.0298	3.896	-3.979	-0.0115	-0.0752	0.0313	-1.593	-8.17	9945

Table 5: Composite three-layered cylinder with [90°/0°/90°] lamination. Comparison of various models for thick cylinders.

		$\hat{w}$	$\hat{\sigma}_{\alpha\alpha}$		$\hat{\sigma}_{\beta\beta}$		$\hat{\sigma}_{\alpha\beta}$		$\hat{\sigma}_{\alpha z}$	$\hat{\sigma}_{\beta z}$	$\hat{\sigma}_{zz}$	$DOFs$
	$z =$	0	$+h/2$	$-h/2$	$+h/2$	$-h/2$	$+h/2$	$-h/2$	$-h/6$	0	0	
$R/h = 10$	3D *Elasticity*[43]	1.223	0.0739	-0.0791	4.683	-5.224	0.0374	-0.0729	0.0826	-3.264	-1.27	
	$LW2_a$[39]	1.223	-	-	-	-	-	-	-	-3.283	-1.24	
	$ESL2_a$[39]	0.944	-	-	-	-	-	-	-	-	-	
	$LW4$	1.223	0.0741	-0.0793	4.698	-5.240	0.0376	-0.0734	0.0829	-3.274	-1.27	43095
	$LW1$	1.190	0.0626	-0.0950	4.456	-4.972	0.0363	-0.0707	0.0717	-3.281	-1.27	13260
	$EL3Z$	1.223	0.0791	-0.0882	4.705	-5.241	0.0376	-0.0733	0.0680	-3.321	-1.30	16575
	$EL4$	1.143	0.0703	-0.0820	4.578	-5.106	0.0363	-0.0692	0.1068	-2.422	-1.35	16575
	$EL1$	0.953	0.0448	-0.0840	3.744	-4.107	0.0303	-0.0566	0.0713	-1.262	-1.08	6630
	$EL4_{Case\,1}$	1.204	0.0733	-0.0784	4.660	-5.206	0.0372	-0.0725	0.1238	-3.280	-1.27	29835
	$EL1_{Case\,1}$	0.985	0.0534	-0.0799	4.123	-3.923	0.0324	-0.0573	0.0738	-1.534	-1.04	9945
	$EL4_{Case\,2}$	1.205	0.0733	-0.0788	4.673	-5.200	0.0374	-0.0723	0.0973	-3.276	-1.27	29835
	$EL1_{Case\,2}$	0.992	0.0387	-0.0886	3.547	-4.578	0.0301	-0.0600	0.0661	-1.584	-1.22	9945
$R/h = 4$	3D *Elasticity*[43]	4.009	0.1270	-0.2701	6.545	-9.323	0.1081	-0.1609	0.1736	-2.349	-0.62	
	$LW2_a$[39]	4.007	-	-	-	-	-	-	-	-2.399	-0.60	
	$ESL2_a$[39]	2.917	-	-	-	-	-	-	-	-	-	
	$LW4$	4.009	0.1271	-0.2725	6.565	-9.354	0.1088	-0.1619	0.1742	-2.356	-0.62	43095
	$LW1$	3.852	0.0826	-0.2772	5.585	-7.702	0.1020	-0.1491	0.1663	-2.360	-0.62	13260
	$EL3Z$	3.970	0.1352	-0.3140	6.519	-9.056	0.1072	-0.1593	0.1496	-2.353	-0.62	16575
	$EL4$	3.772	0.1124	-0.3026	6.342	-9.094	0.1050	-0.1545	0.2332	-1.936	-0.67	16575
	$EL1$	3.004	-0.0052	-0.1676	3.210	-4.024	0.0787	-0.1085	0.1512	-1.147	-0.62	6630
	$EL4_{Case\,1}$	3.917	0.1244	-0.2796	6.434	-9.155	0.1065	-0.1594	0.2708	-2.269	-0.59	29835
	$EL1_{Case\,1}$	3.084	0.0549	-0.1711	4.505	-3.311	0.0839	-0.1085	0.1571	-1.272	-0.72	9945
	$EL4_{Case\,2}$	3.940	0.1232	-0.2706	6.475	-9.213	0.1079	-0.1588	0.2078	-2.305	-0.62	29835
	$EL1_{Case\,2}$	3.151	-0.0065	-0.2510	2.334	-6.233	0.0768	-0.1201	0.1484	-1.389	-0.54	9945
$R/h = 2$	3D *Elasticity*[43]	10.11	0.1761	-0.8428	7.168	-18.19	0.1797	-0.2922	0.3006	-1.379	-0.34	
	$LW2_a$[39]	10.33	-	-	-	-	-	-	-	-1.421	-0.33	
	$ESL2_a$[39]	8.95	-	-	-	-	-	-	-	-	-	
	$LW4$	10.10	0.1741	-0.8730	7.179	-18.17	0.1807	-0.2934	0.3018	-1.382	-0.34	43095
	$LW1$	9.51	0.0738	-0.6604	5.079	-10.67	0.1630	-0.2339	0.2974	-1.328	-0.33	13260
	$EL3Z$	9.65	0.1487	-0.8951	6.848	-14.15	0.1728	-0.2653	0.2679	-1.294	-0.32	16575
	$EL4$	9.59	0.1425	-0.9572	6.568	-15.63	0.1775	-0.2783	0.4244	-1.219	-0.35	16575
	$EL1$	8.82	-0.1046	-0.3218	2.441	-3.79	0.1542	-0.2152	0.2941	-0.927	-0.37	6630
	$EL4_{Case\,1}$	9.80	0.1690	-0.9187	6.955	-16.58	0.1756	-0.2859	0.4837	-1.191	-0.30	29835
	$EL1_{Case\,1}$	8.48	0.0335	-0.3866	3.356	-3.10	0.1391	-0.2029	0.3104	-0.875	-0.50	9945
	$EL4_{Case\,2}$	9.97	0.1703	-0.8701	6.931	-17.98	0.1798	-0.2894	0.3561	-1.318	-0.34	29835
	$EL1_{Case\,2}$	8.71	-0.0647	-0.6301	0.711	-8.71	0.1380	-0.2087	0.2700	-1.031	-0.26	9945

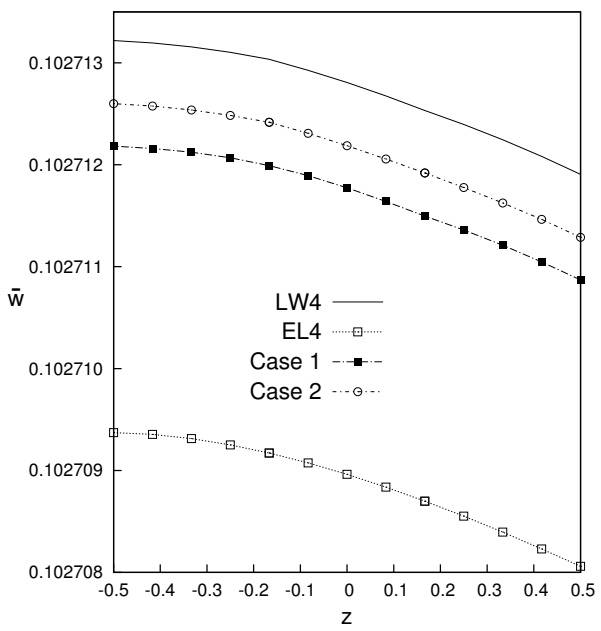

Figure 7: Composite three-layered cylinder. Transverse displacement w along the thickness. Radius-to-thickness ratio $(\,R\,/\,h\,) = 500$.

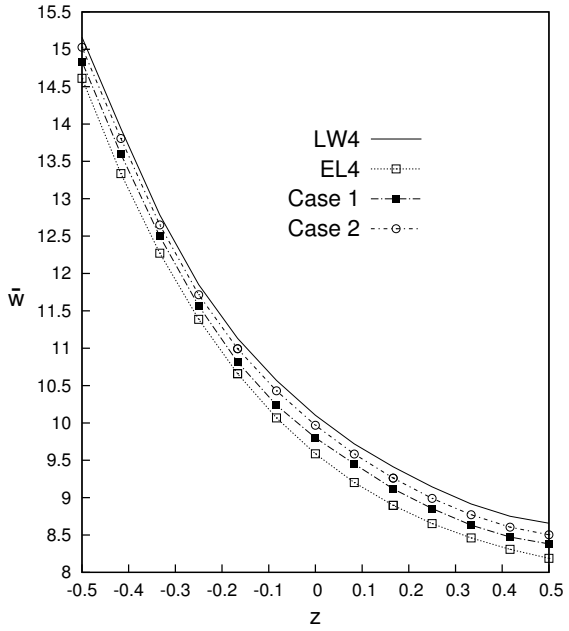

Figure 8: Composite three-layered cylinder. Transverse displacement w along the thickness. Radius-to-thickness ratio $(\,R\,/\,h\,) = 2$.

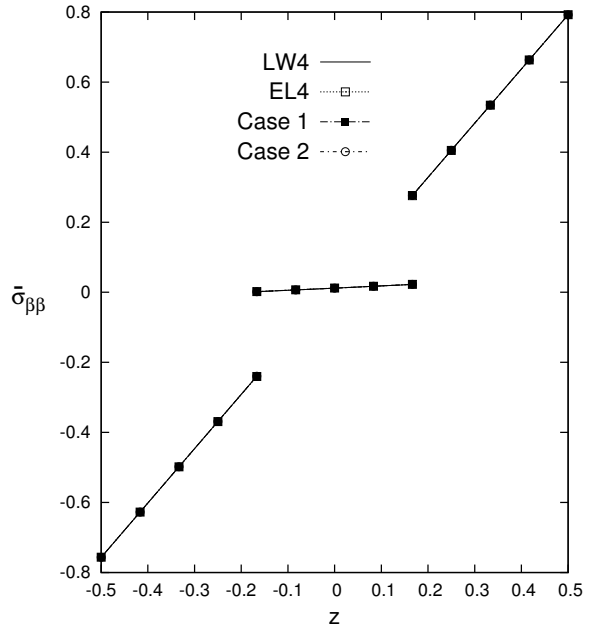

Figure 9: Composite three-layered cylinder. In-plane stress $\sigma_{\beta\beta}$ along the thickness. Radius-to-thickness ratio $(\,R\,/\,h\,) = 500$.

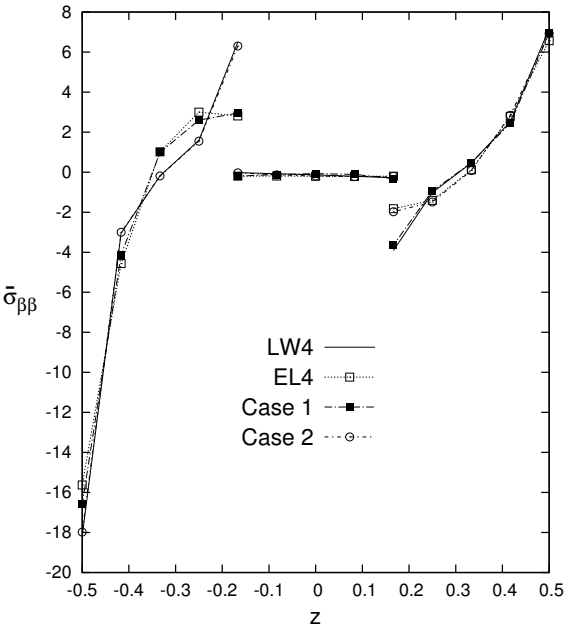

Figure 10: Composite three-layered cylinder. In-plane stress $\sigma_{\beta\beta}$ along the thickness. Radius-to-thickness ratio $(\,R\,/\,h\,) = 2$.

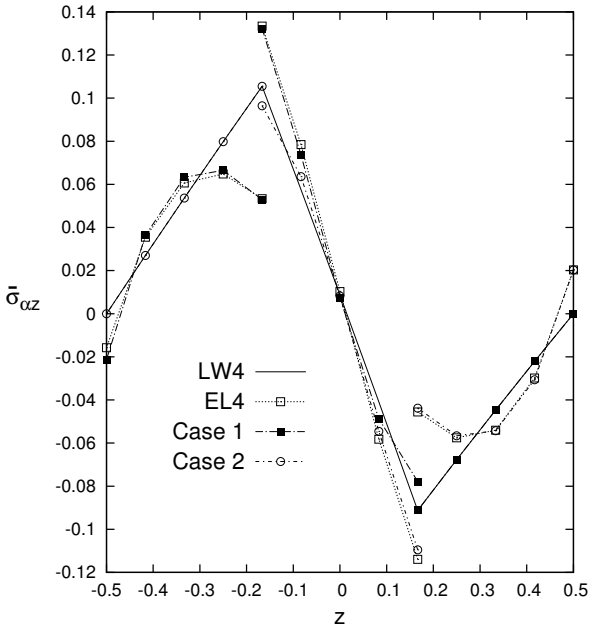

Figure 11: Composite three-layered cylinder. Transverse shear stress $\sigma_{\alpha z}$ along the thickness. Radius-to-thickness ratio $(R / h) = 500$.

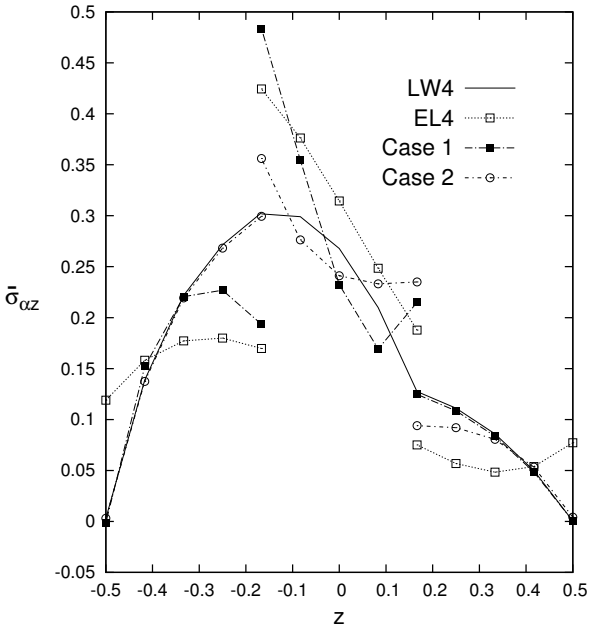

Figure 12: Composite three-layered cylinder. Transverse shear stress $\sigma_{\alpha z}$ along the thickness. Radius-to-thickness ratio $(R / h) = 2$.

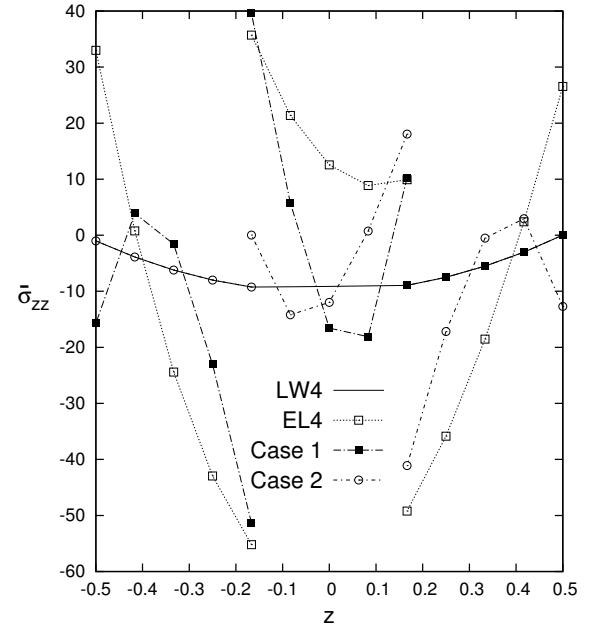

Figure 13: Composite three-layered cylinder. Transverse normal stress σ_{zz} along the thickness. Radius-to-thickness ratio $(R / h) = 500$.

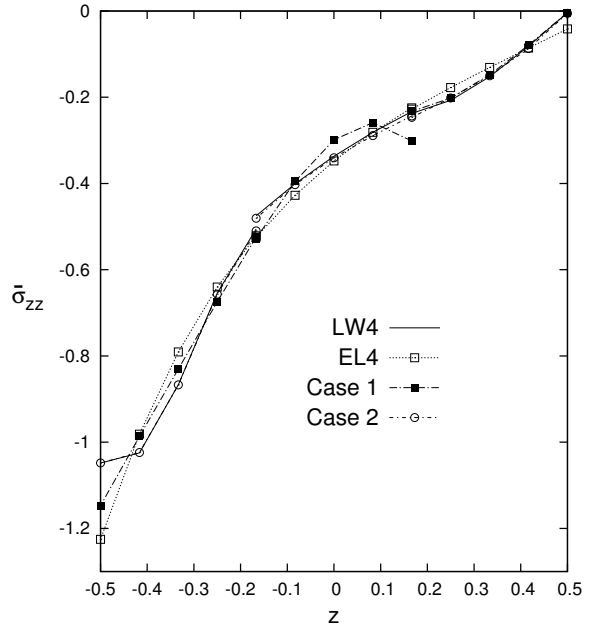

Figure 14: Composite three-layered cylinder. Transverse normal stress σ_{zz} along the thickness. Radius-to-thickness ratio $(R / h) = 2$.

6.2 Ten-layer composite cylinder

As a second assessment, a ten-layer cross-ply cylinder with lamination $(90°/0°/90°/0°/90°)_S$ and simply-supported boundary condition is considered. The geometrical and material data and the applied

load at the inner surface of the shell are the same as those defined for the previous analysis case. Also, because of the geometrical symmetry of the cylinder, the symmetry of the load pressure and boundary condition, and the symmetry of the lamination stacking sequence, only one octave of the cylinder is analysed. A mesh grid of 8×32 elements is used, as in the case of the three-layered cylinder of the previous section.

Different variable kinematic models are employed to show the global/local capabilities of the present CUF-based methodology. Depending on the sublaminates grouping, the acronyms have been modified adding a subscript to them in the case of variable kinematics. The list of subscripts is given below for the sake of completeness:

- $Case\,1 = \{layer1\}\,\{layer2, layer3, layer4, layer5, layer6, layer7, layer8, layer9\}\,\{layer10\}$
- $Case\,2 = \{layer1, layer2\}\,\{layer3, layer4, layer5, layer6, layer7, layer8\}\,\{layer9, layer10\}$
- $Case\,3 = \{layer1, layer2, layer3\}\,\{layer4, layer5, layer6, layer7\}\,\{layer8, layer9, layer10\}$
- $Case\,4 = \{layer1, layer2, layer3, layer4\}\,\{layer5, layer6\}\,\{layer7, layer8, layer9, layer10\}$
- $Case\,5 = \{layer1\}\,\{layer2, layer3\}\,\{layer4, layer5, layer6, layer7\}\,\{layer8, layer9\}\,\{layer10\}$
- $Case\,6 = \{layer1\}\,\{layer2, layer3, layer4\}\,\{layer5, layer6\}\,\{layer7, layer8, layer9\}\,\{layer10\}$

The results from the present models are reported in non-dimensional form, as in the previous case, and they are listed in Tables 6 and 7 and Figs. 16 to 22 for various radius-to-thickness ratios R/h. The present FEM results are compared with those from 3D elasticity solution [43] and a layer-wise analytical model [39]. The following comments can be made from the analysis of the results

- Regarding the transverse displacement w, all the variable-kinematic models lead a significant improvement of the solution with respect to $EL4$ and for every radius-to-thickness ratios, see Figs. 15 and 16.
- As in the previous analysis case and according to Fig. 17, no accuracy differences are appreciable in terms of in-plane stress $\sigma_{\beta\beta}$ between the various models of the thin cylinders. Conversely, for small ratios $R/h = 2$, the theories $EL4_{,Case1}$, $EL4_{,Case4}$ and $EL4_{,Case6}$ improve the results with respect to the global $EL4$ model, especially in the layers that have a layer-wise assembling, see Fig. 18.
- In the case of shear stress $\sigma_{\alpha z}$ and variable kinematic models, the results reach the exact solution in the layers that have a layer-wise assembling for both thin and thick cylinders. On the contrary, the remaining layers with an equivalent-single-layer assembling have a loss of accuracy, see Figs. 19 and 20.
- As far as the transverse normal stress σ_{zz} is concerned and for large ratios $R/h = 500$, the variable kinematics results reach the exact and full LW solutions in the layers that have a layer-wise assembling, see Fig. 21. On the other hand, Fig. 22 shows that the shell theory $EL4_{,Case6}$ approximates very well the layer-wise solution along the thickness in the case of thin structures.

Table 6: Composite ten-layered cylinder with $[90°/0°/90°/0°/90°]_S$ lamination. Comparison of various models for thin cylinders.

		$\hat{w}$	$\hat{\sigma}_{\alpha\alpha}$		$\hat{\sigma}_{\beta\beta}$		$\hat{\sigma}_{\alpha\beta}$		$\hat{\sigma}_{\alpha z}$	$\hat{\sigma}_{\beta z}$	$\hat{\sigma}_{zz}$	$DOFs$
	$z =$	0	$+h/2$	$-h/2$	$+h/2$	$-h/2$	$+h/2$	$-h/2$	0	0	0	
$R/h = 500$	3D *Elasticity*[43]	0.1006	0.0516	0.0340	0.7770	-0.7351	-0.0829	-0.0949	0.0102	-0.4670	-6.32	
	$LW4$	0.1006	0.0518	0.0341	0.7795	-0.7374	-0.0834	-0.0956	0.0103	-0.4685	-6.33	135915
	$LW1$	0.1006	0.0520	0.0338	0.7798	-0.7378	-0.0834	-0.0956	0.0264	-0.4587	-32.36	36465
	$EL3Z$	0.1006	0.0517	0.0338	0.7794	-0.7377	-0.0834	-0.0956	0.0057	-0.6194	-49.00	16575
	$EL4$	0.1006	0.0516	0.0339	0.7793	-0.7376	-0.0834	-0.0956	0.0065	-0.6196	-37.69	16575
	$EL1$	0.1005	0.0541	0.0311	0.7819	-0.7404	-0.0834	-0.0955	0.0044	-0.4438	-31.93	6630
	$EL4_{Case\,1}$	0.1006	0.0518	0.0341	0.7795	-0.7374	-0.0834	-0.0956	0.0069	-0.5528	-24.37	43095
	$EL4_{Case\,2}$	0.1006	0.0517	0.0339	0.7794	-0.7376	-0.0834	-0.0956	0.0064	-0.6123	-35.38	43095
	$EL4_{Case\,3}$	0.1006	0.0519	0.0346	0.7797	-0.7369	-0.0834	-0.0956	0.0091	-0.4281	-8.35	43095
	$EL4_{Case\,4}$	0.1006	0.0520	0.0346	0.7797	-0.7368	-0.0834	-0.0956	0.0103	-0.4685	-6.33	43095
	$EL4_{Case\,5}$	0.1006	0.0518	0.0341	0.7795	-0.7374	-0.0834	-0.0956	0.0091	-0.4281	-8.35	69615
	$EL4_{Case\,6}$	0.1006	0.0518	0.0341	0.7795	-0.7374	-0.0834	-0.0956	0.0103	-0.4685	-6.33	69615
$R/h = 100$	3D *Elasticity*[43]	0.6261	0.1076	-0.0015	4.677	-4.670	-0.0734	-0.1479	0.0631	-2.884	-7.69	
	$LW2_a$[39]	0.6261	-	-	-	-	-	-	-	-2.884	-7.69	
	$ESL2_a$[39]	0.6252	-	-	-	-	-	-	-	-	-	
	$LW4$	0.6261	0.1080	-0.0016	4.692	-4.685	-0.0738	-0.1489	0.0634	-2.893	-7.71	135915
	$LW1$	0.6261	0.1090	-0.0038	4.693	-4.687	-0.0738	-0.1489	0.0831	-2.830	-13.96	36465
	$EL3Z$	0.6254	0.1079	-0.0027	4.693	-4.686	-0.0737	-0.1487	0.0393	-3.830	-12.10	16575
	$EL4$	0.6254	0.1075	-0.0022	4.692	-4.686	-0.0737	-0.1487	0.0402	-3.827	-9.29	16575
	$EL1$	0.6221	0.1218	-0.0195	4.689	-4.681	-0.0733	-0.1480	0.0269	-2.732	-7.02	6630
	$EL4_{Case\,1}$	0.6255	0.1079	-0.0016	4.692	-4.685	-0.0737	-0.1487	0.0424	-3.414	-8.53	43095
	$EL4_{Case\,2}$	0.6255	0.1082	-0.0021	4.692	-4.685	-0.0737	-0.1488	0.0393	-3.782	-9.19	43095
	$EL4_{Case\,3}$	0.6259	0.1075	-0.0002	4.692	-4.683	-0.0738	-0.1488	0.0560	-2.643	-7.67	43095
	$EL4_{Case\,4}$	0.6258	0.1072	-0.0003	4.692	-4.683	-0.0738	-0.1488	0.0634	-2.893	-7.71	43095
	$EL4_{Case\,5}$	0.6260	0.1079	-0.0016	4.692	-4.685	-0.0738	-0.1488	0.0560	-2.643	-7.67	69615
	$EL4_{Case\,6}$	0.6259	0.1079	-0.0016	4.692	-4.685	-0.0738	-0.1488	0.0634	-2.893	-7.71	69615
$R/h = 50$	3D *Elasticity*[43]	0.7622	0.0971	-0.0340	5.529	-5.606	-0.0223	-0.1120	0.0760	-3.425	-4.76	
	$LW2_a$[39]	0.7622	-	-	-	-	-	-	-	-3.425	-4.76	
	$ESL2_a$[39]	0.7564	-	-	-	-	-	-	-	-	-	
	$LW4$	0.7622	0.0974	-0.0341	5.546	-5.624	-0.0225	-0.1128	0.0763	-3.436	-4.77	135915
	$LW1$	0.7620	0.0980	-0.0374	5.545	-5.626	-0.0225	-0.1127	0.0880	-3.360	-6.54	36465
	$EL3Z$	0.7580	0.0972	-0.0358	5.544	-5.624	-0.0222	-0.1123	0.0477	-4.553	-5.86	16575
	$EL4$	0.7580	0.0965	-0.0351	5.543	-5.623	-0.0222	-0.1123	0.0483	-4.545	-5.02	16575
	$EL1$	0.7517	0.1118	-0.0563	5.524	-5.599	-0.0220	-0.1113	0.0321	-3.243	-3.77	6630
	$EL4_{Case\,1}$	0.7585	0.0972	-0.0342	5.543	-5.621	-0.0222	-0.1123	0.0508	-4.055	-4.86	43095
	$EL4_{Case\,2}$	0.7589	0.0977	-0.0346	5.543	-5.620	-0.0223	-0.1124	0.0472	-4.492	-5.01	43095
	$EL4_{Case\,3}$	0.7607	0.0967	-0.0327	5.546	-5.623	-0.0224	-0.1126	0.0673	-3.139	-4.70	43095
	$EL4_{Case\,4}$	0.7604	0.0962	-0.0330	5.546	-5.624	-0.0223	-0.1125	0.0761	-3.436	-4.77	43095
	$EL4_{Case\,5}$	0.7614	0.0974	-0.0341	5.546	-5.623	-0.0224	-0.1127	0.0673	-3.140	-4.70	69615
	$EL4_{Case\,6}$	0.7611	0.0974	-0.0341	5.546	-5.624	-0.0224	-0.1126	0.0762	-3.436	-4.77	69615

Table 7: Composite ten-layered cylinder with $[90°/0°/90°/0°/90°]_S$ lamination. Comparison of various models for thick cylinders.

		$\hat{w}$	$\hat{\sigma}_{\alpha\alpha}$		$\hat{\sigma}_{\beta\beta}$		$\hat{\sigma}_{\alpha\beta}$		$\hat{\sigma}_{\alpha z}$	$\hat{\sigma}_{\beta z}$	$\hat{\sigma}_{zz}$	$DOFs$
	$z =$	0	$+h/2$	$-h/2$	$+h/2$	$-h/2$	$+h/2$	$-h/2$	0	0	0	
$R/h = 10$	$3D$ *Elasticity*[43]	1.380	0.0877	-0.0927	5.875	-6.462	0.0406	-0.0869	0.1084	-3.479	-1.32	
	$LW2_a$[39]	1.380	-	-	-	-	-	-	-	-3.475	-1.32	
	$ESL2_a$[39]	1.200	-	-	-	-	-	-	-	-	-	
	$LW4$	1.380	0.0879	-0.0929	5.893	-6.483	0.0408	-0.0874	0.1087	-3.490	-1.32	135915
	$LW1$	1.375	0.0835	-0.1029	5.855	-6.453	0.0407	-0.0870	0.1127	-3.395	-1.32	36465
	$EL3Z$	1.265	0.0856	-0.1007	5.795	-6.382	0.0397	-0.0819	0.0656	-4.624	-1.37	16575
	$EL4$	1.265	0.0806	-0.0958	5.788	-6.380	0.0397	-0.0820	0.0656	-4.584	-1.33	16575
	$EL1$	1.205	0.0715	-0.1102	5.420	-5.947	0.0375	-0.0771	0.0415	-3.309	-1.09	6630
	$EL4_{Case\,1}$	1.282	0.0849	-0.0914	5.778	-6.352	0.0397	-0.0826	0.0698	-4.095	-1.31	43095
	$EL4_{Case\,2}$	1.293	0.0860	-0.0909	5.772	-6.339	0.0398	-0.0831	0.0650	-4.547	-1.33	43095
	$EL4_{Case\,3}$	1.339	0.0876	-0.0913	5.895	-6.490	0.0406	-0.0857	0.0944	-3.167	-1.30	43095
	$EL4_{Case\,4}$	1.330	0.0853	-0.0937	5.888	-6.490	0.0405	-0.0853	0.1060	-3.471	-1.32	43095
	$EL4_{Case\,5}$	1.357	0.0873	-0.0927	5.872	-6.458	0.0407	-0.0864	0.0955	-3.179	-1.30	69615
	$EL4_{Case\,6}$	1.351	0.0872	-0.0927	5.877	-6.467	0.0406	-0.0861	0.1074	-3.485	-1.32	69615
$R/h = 4$	$3D$ *Elasticity*[43]	4.206	0.1243	-0.2674	6.635	-8.970	0.0972	-0.1652	0.2117	-3.154	-0.71	
	$LW2_a$[39]	4.206	-	-	-	-	-	-	-	-3.137	-0.71	
	$ESL2_a$[39]	3.240	-	-	-	-	-	-	-	-	-	
	$LW4$	4.206	0.1247	-0.2678	6.656	-8.998	0.0978	-0.1663	0.2124	-3.164	-0.71	135915
	$LW1$	4.175	0.1116	-0.2913	6.473	-8.712	0.0967	-0.1640	0.2161	-3.027	-0.65	36465
	$EL3Z$	3.566	0.1177	-0.2955	6.215	-8.109	0.0900	-0.1457	0.1239	-4.053	-0.70	16575
	$EL4$	3.563	0.0957	-0.2771	6.128	-8.231	0.0898	-0.1465	0.1236	-3.952	-0.70	16575
	$EL1$	3.335	0.0136	-0.1942	4.635	-5.818	0.0817	-0.1241	0.0748	-3.012	-0.63	6630
	$EL4_{Case\,1}$	3.705	0.1150	-0.2600	6.223	-8.394	0.0917	-0.1510	0.1347	-3.578	-0.70	43095
	$EL4_{Case\,2}$	3.768	0.1161	-0.2583	6.202	-8.358	0.0923	-0.1529	0.1256	-4.003	-0.70	43095
	$EL4_{Case\,3}$	3.973	0.1243	-0.2700	6.635	-8.997	0.0958	-0.1602	0.1825	-2.791	-0.69	43095
	$EL4_{Case\,4}$	3.923	0.1210	-0.2755	6.614	-8.979	0.0952	-0.1589	0.2020	-3.079	-0.70	43095
	$EL4_{Case\,5}$	4.088	0.1227	-0.2663	6.572	-8.876	0.0968	-0.1631	0.1873	-2.842	-0.70	69615
	$EL4_{Case\,6}$	4.052	0.1224	-0.2664	6.584	-8.893	0.0966	-0.1623	0.2082	-3.137	-0.71	69615
$R/h = 2$	$3D$ *Elasticity*[43]	11.44	0.1691	-0.8532	7.202	-18.31	0.1545	-0.3363	0.3019	-2.608	-0.42	
	$LW2_a$[39]	11.44	-	-	-	-	-	-	-	-2.581	-0.42	
	$ESL2_a$[39]	9.39	-	-	-	-	-	-	-	-	-	
	$LW4$	11.44	0.1696	-0.8554	7.225	-18.37	0.1555	-0.3384	0.3029	-2.618	-0.42	135915
	$LW1$	11.28	0.1442	-0.8850	6.750	-16.42	0.1518	-0.3265	0.3062	-2.426	-0.36	36465
	$EL3Z$	9.42	0.1369	-0.8804	6.101	-11.96	0.1418	-0.2877	0.1876	-3.039	-0.39	16575
	$EL4$	9.39	0.0967	-0.8775	5.485	-13.08	0.1382	-0.2952	0.1874	-2.820	-0.39	16575
	$EL1$	9.46	-0.1091	-0.3480	3.509	-5.46	0.1368	-0.2097	0.1245	-2.449	-0.39	6630
	$EL4_{Case\,1}$	10.13	0.1561	-0.8409	6.555	-17.04	0.1484	-0.3205	0.2095	-2.671	-0.40	43095
	$EL4_{Case\,2}$	10.31	0.1562	-0.8490	6.528	-17.12	0.1494	-0.3243	0.1912	-3.009	-0.40	43095
	$EL4_{Case\,3}$	10.76	0.1675	-0.8962	7.109	-18.21	0.1527	-0.3305	0.2666	-2.229	-0.40	43095
	$EL4_{Case\,4}$	10.61	0.1667	-0.9099	7.081	-18.14	0.1524	-0.3312	0.2911	-2.484	-0.41	43095
	$EL4_{Case\,5}$	11.11	0.1666	-0.8518	7.067	-18.03	0.1544	-0.3340	0.2739	-2.298	-0.41	69615
	$EL4_{Case\,6}$	11.02	0.1665	-0.8519	7.072	-17.99	0.1548	-0.3351	0.3006	-2.568	-0.42	69615

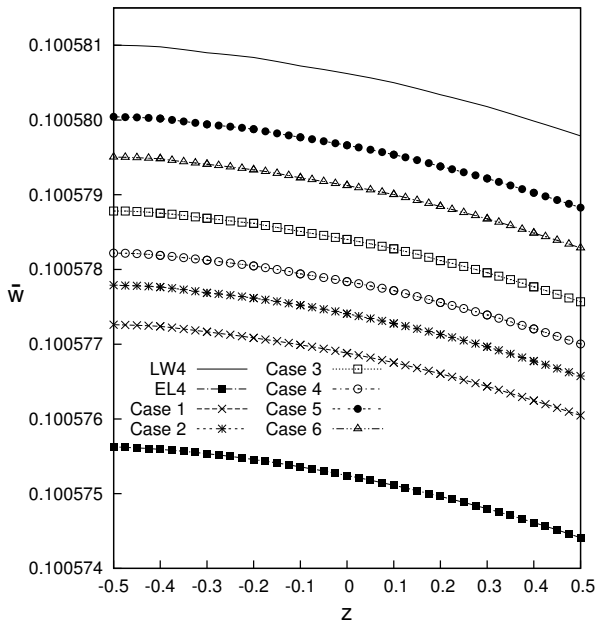

Figure 15: Composite ten-layered cylinder. Transverse displacement w along the thickness. Radius-to-thickness ratio $(\,R\,/\,h\,) = 500$.

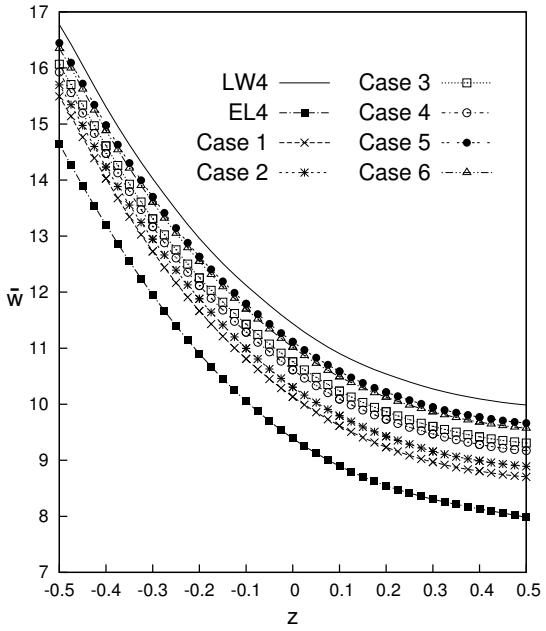

Figure 16: Composite ten-layered cylinder. Transverse displacement w along the thickness. Radius-to-thickness ratio $(\,R\,/\,h\,) = 2$.

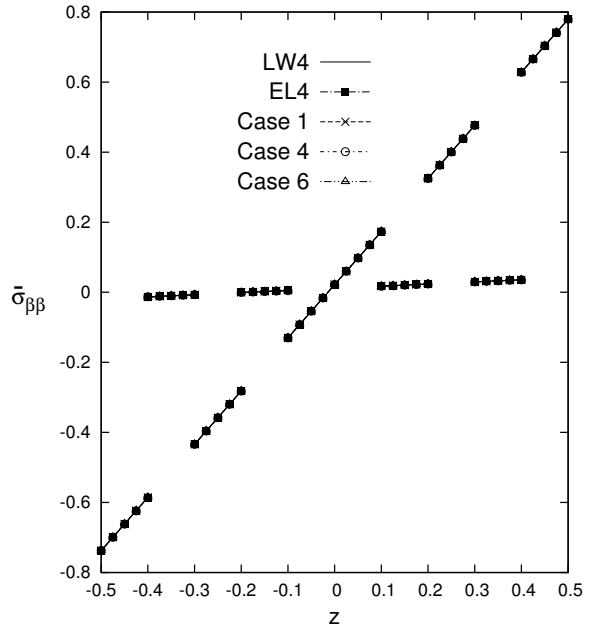

Figure 17: Composite ten-layered cylinder. In-plane stress $\sigma_{\beta\beta}$ along the thickness. Radius-to-thickness ratio $(\,R\,/\,h\,) = 500$.

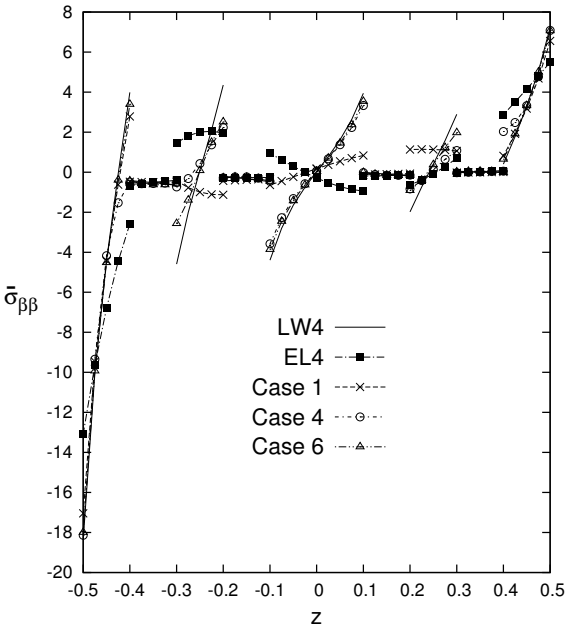

Figure 18: Composite ten-layered cylinder. In-plane stress $\sigma_{\beta\beta}$ along the thickness. Radius-to-thickness ratio $(\,R\,/\,h\,) = 2$.

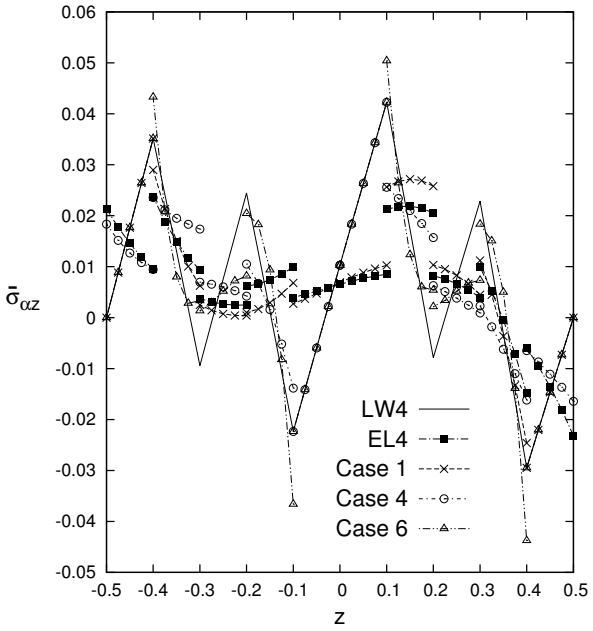

Figure 19: Composite ten-layered cylinder. Transverse shear stress $\sigma_{\alpha z}$ along the thickness. Radius-to-thickness ratio $(R / h) = 500$.

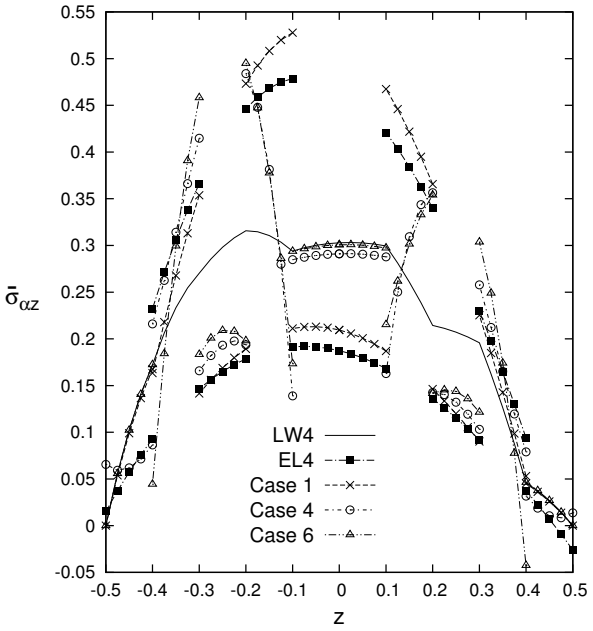

Figure 20: Composite ten-layered cylinder. Transverse shear stress $\sigma_{\alpha z}$ along the thickness. Radius-to-thickness ratio $(R / h) = 2$.

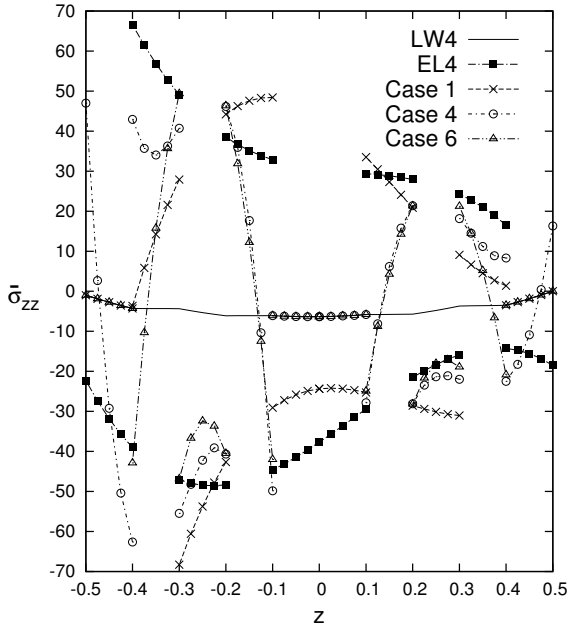

Figure 21: Composite ten-layered cylinder. Transverse normal stress σ_{zz} along the thickness. Radius-to-thickness ratio $(R / h) = 500$.

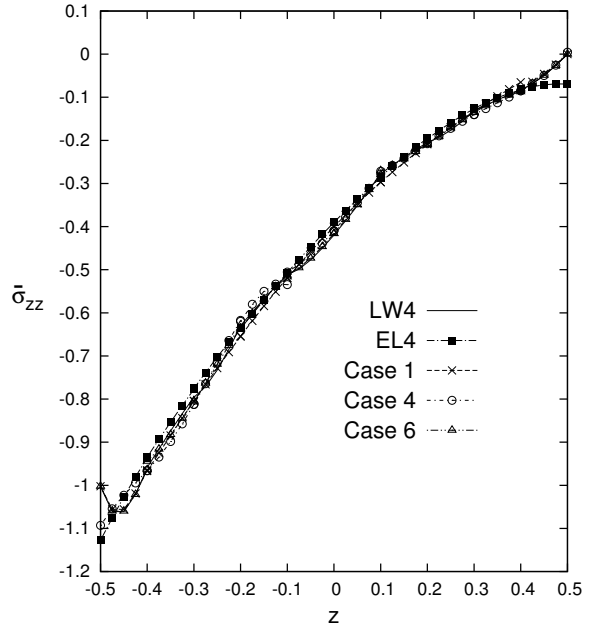

Figure 22: Composite ten-layered cylinder. Transverse normal stress σ_{zz} along the thickness. Radius-to-thickness ratio $(R / h) = 2$.

6.3 Composite spherical panel

A preliminary analysis of cross-ply spherical panels with (0°/90°/0°) and (0°/90°/90°/0°) laminations and simply-supported boundary conditions are considered next. The load is a pressure applied at the

outer surface of the shell and it is defined as follows:

$$p\left(\alpha,\beta,z_{top}\right)=\hat{p}\,sin\left(\frac{m\pi\alpha}{a}\right)sin\left(\frac{n\pi\beta}{b}\right) \tag{24}$$

where $\hat{p}=1.0$, $m=1$ and $n=1$. The mechanical properties of the material are: $E_L/E_T=25$; $G_{LT}/E_T=0.5$; $G_{TT}/E_T=0.2$; $\nu_{LT}=\nu_{TT}=0.25$. Different radius-to-side length ratios $R/a=$ 5, 10, 50, 100 and different side length-to-thickness ratios $a/h=10$, 100 are considered. The panel is square such that $a/b=1$ and $R_\alpha/R_\beta=1$. The layers are of equal thickness and $h_{total}=1.0$. The results are given in terms of transverse displacements and reported in non-dimensional form as follows:

$$\hat{w}=-\frac{10^3\,w\,E_T\,h^3}{\hat{p}\,a^4}\qquad\qquad\hat{\sigma}_{\alpha z}=\frac{10^4\sigma_{\alpha z}}{\hat{p}(R/h)}\qquad\qquad\hat{\sigma}_{zz}=\frac{\sigma_{zz}}{\hat{p}}$$

Even for this analysis case, different variable kinematic models are used to perform the analysis of the shell structures. Usual acronyms are enriched with the following subscripts which indicate the sublaminates grouping. For the three-layered spherical shell we consider

- $Case1=\{layer1\}\,\{layer2,layer3\}$
- $Case2=\{layer1,layer2\}\,\{layer3\}$

On the other hand, for the four-layered shell we have

- $Case1=\{layer1\}\,\{layer2,layer3,layer4\}$
- $Case2=\{layer1,layer2,layer3\}\,\{layer4\}$
- $Case3=\{layer1,layer2\}\,\{layer3,layer4\}$
- $Case4=\{layer1\}\,\{layer2,layer3\}\,\{layer4\}$

First, a convergence study on the shell element was performed. A composite shell with radius to side length ratio $R/a=10$ and side length to thickness ratio $a/h=10$ is considered for this purpose. As demonstrated in Table 8 in the case of a full LW model, a mesh grid of 12×12 elements ensures the convergence. The results from the other full kinematic and variable kinematic models are reported in non-dimensional form for the transverse displcament in Table 9, and for the transverse shear and normal stresses in Table 10 for different thickness ratios a/h and radius-to-side length ratio R/a. The present FEM results are compared with higher-order models from the literature, i.e. [44] and [45], and a layer-wise analytical model by Carrera [39]. It can be observed that changing the R/a ratio, the transverse displacement variation is higher for thin shells with ratio $a/h=100$ than for thick shells with ratio $a/h=10$. Therefore it can be seen that the best approximation compromise is given by the theory $EL4_{,Case1}$, where the loaded layer is described by a layer-wise model and the remaining layers are described by equivalent single layer approach. For the four-layered shell, the theory $EL4_{,Case4}$ is more accurate then $EL4_{,Case1}$ model. This is due only to the fact that a symmetric lamination scheme is considered.

Table 8: Convergence study. Composite spherical panel with lamination [0°/90°/0°]. Radius-to-side length ratio $R/a=10$ and side length-to-thickness ratio $a/h=10$.

	Mesh	4×4	6×6	8×8	10×10	12×12
$LW4$	$\hat{w}\ (z=0)$	7.5175	7.5129	7.5121	7.5118	7.5117

Table 9: Composite spherical panel with $[0°/90°/0°]$ and $[0°/90°/90°/0°]$ laminations. Transverse displacement $\hat{w} = \hat{w}(a/2, b/2, 0)$. Results presented for different R/a and a/h ratios.

		$a/h = 10$				$a/h = 100$				
	R/a	5	10	50	100	5	10	50	100	$DOFs$
3 Layers	$HSDT^1$[44]	6.7688	7.0325	7.1212	7.1240	1.0321	2.4099	4.2071	4.3074	
	$HSDT^2$[45]	6.8201	7.0459	7.1213	7.1237	1.0321	2.4020	4.1249	4.2603	
	$LW2_a$[39]	7.121	7.392		7.504					
	$LW4$	7.3252	7.5117	7.5408	7.5365	1.0364	2.4166	4.2132	4.3131	24375
	$LW1$	7.1793	7.3568	7.3835	7.3792	1.0360	2.4143	4.2061	4.3057	7500
	$EL3Z$	7.3219	7.5089	7.5382	7.5339	1.0364	2.4166	4.2132	4.3131	9375
	$EL4$	6.9739	7.1376	7.1606	7.1564	1.0362	2.4152	4.2087	4.3085	9375
	$EL1$	6.1234	6.2381	6.2489	6.2450	1.0327	2.3962	4.1514	4.2485	3750
	$EL4_{Case\,1}$	7.2331	7.4092	7.4327	7.4279	1.0364	2.4163	4.2121	4.3120	16875
	$EL4_{Case\,2}$	7.2309	7.4080	7.4324	7.4278	1.0364	2.4163	4.2121	4.3120	16875
4 Layers	$HSDT^1$[44]	6.7865	7.0536	7.1436	7.1464	1.0264	2.4024	4.2071	4.3082	
	$HSDT^2$[45]	6.8380	7.0670	7.1436	7.1459	1.0254	2.3866	4.1284	4.2418	
	$LW4$	7.1738	7.3528	7.3801	7.3758	1.0306	2.4083	4.2111	4.3117	31875
	$LW1$	7.0820	7.2554	7.2811	7.2769	1.0303	2.4070	4.2071	4.3075	9375
	$EL3Z$	6.9973	7.1651	7.1894	7.1852	1.0304	2.4076	4.2088	4.3093	9375
	$EL4$	6.9971	7.1648	7.1891	7.1849	1.0304	2.4076	4.2088	4.3093	9375
	$EL1$	6.0771	6.1912	6.2020	6.1982	1.0269	2.3884	4.1503	4.2480	3750
	$EL4_{Case\,1}$	7.1141	7.2877	7.3127	7.3083	1.0305	2.4081	4.2103	4.3108	16875
	$EL4_{Case\,2}$	7.1086	7.2850	7.3124	7.3083	1.0305	2.4080	4.2102	4.3108	16875
	$EL4_{Case\,3}$	7.0925	7.2663	7.2921	7.2879	1.0305	2.4080	4.2100	4.3106	16875
	$EL4_{Case\,4}$	7.1738	7.3528	7.3801	7.3758	1.0306	2.4083	4.2111	4.3117	24375

Table 10: Composite spherical panel with $[0°/90°/0°]$ and $[0°/90°/90°/0°]$ laminations. Transverse shear stress $\hat{\sigma}_{\alpha z} = \hat{\sigma}_{\alpha z}(a/2, b/2, 0)$, and transverse normal stress $\hat{\sigma}_{zz} = \hat{\sigma}_{\alpha z}(a/2, b/2, +h/2)$. Results presented for different R/a and a/h ratios.

		$a/h = 10$				$a/h = 100$				
		$\hat{\sigma}_{\alpha z}$		$\hat{\sigma}_{zz}$		$\hat{\sigma}_{\alpha z}$		$\hat{\sigma}_{zz}$		
	R/a	5	100	5	100	5	100	5	100	$DOFs$
3 Layers	$LW4$	-0.4909	-0.0254	-1.0003	-1.0005	-0.1270	-0.0308	-1.0041	-1.0125	24375
	$LW1$	-0.5225	-0.0270	-1.3539	-1.5057	-0.1295	-0.0312	-10.839	-43.924	7500
	$EL3Z$	-0.5328	-0.0276	-1.2200	-1.2358	-0.1350	-0.0323	-1.0997	-1.2631	9375
	$EL4$	-0.3635	-0.0188	-1.0383	-1.0505	-0.0911	-0.0231	-1.2561	-1.1229	9375
	$EL1$	-0.1581	-0.0081	-1.7265	-1.9412	-0.0215	-0.0082	-30.651	-127.85	3750
	$EL4_{Case\,1}$	-0.4928	-0.0255	-1.0003	-1.0005	-0.1297	-0.0320	-1.0041	-1.0125	16875
	$EL4_{Case\,2}$	-0.4946	-0.0255	-0.9581	-0.9690	-0.1387	-0.0321	-0.8627	-0.9513	16875
4 Layers	$LW4$	-0.4156	-0.0215	-1.0003	-1.0003	-0.1014	-0.0263	-1.0041	-1.0127	31875
	$LW1$	-0.4250	-0.0217	-1.2889	-1.4107	-0.1204	-0.0277	-8.3048	-33.237	9375
	$EL3Z$	-0.4070	-0.0209	-1.2260	-1.2282	-0.1043	-0.0254	-1.0603	-1.2434	9375
	$EL4$	-0.3942	-0.0204	-1.0547	-1.0545	-0.0979	-0.0255	-1.0206	-1.0782	9375
	$EL1$	-0.1616	-0.0083	-1.6803	-1.8929	-0.0202	-0.0086	-30.687	-127.84	3750
	$EL4_{Case\,1}$	-0.4406	-0.0228	-1.0003	-1.0003	-0.1093	-0.0288	-1.0041	-1.0127	16875
	$EL4_{Case\,2}$	-0.4433	-0.0228	-0.9935	-1.0043	-0.1192	-0.0289	-1.0082	-1.0272	16875
	$EL4_{Case\,3}$	-0.3894	-0.0202	-0.9690	-0.9760	-0.0647	-0.0222	-0.9956	-0.9831	16875
	$EL4_{Case\,4}$	-0.4157	-0.0215	-1.0003	-1.0003	-0.1011	-0.0262	-1.0041	-1.0127	24375

6.4 Eleven-layer sandwich cylindrical panel

An eleven-layer simply-supported sandwich cylindrical panel with $(0°/90°/0°/Core/0°/\,90°/0°/Core/0°/90°/0°)$ lamination and simply-supported boundary condition is considered. The load is a pressure applied at the outer surface of the shell, and it is defined as follows:

$$p\,(\alpha, \beta, z_{top}) = \hat{p}\, sin\left(\frac{m\pi\alpha}{a}\right) sin\left(\frac{n\pi\beta}{b}\right) \tag{25}$$

where $m = 1$ and $n = 1$, whereas $\hat{p} = 1.0$. Different axis length-to-circumferential length ratios $b/a = 1, 2$ and circumferential length-to-thickness ratios $a/h = 5, 10$ are considered. The radius-to-circumferential length ratio is fixed for all the cases and it is assumed to be equal to $R_\alpha/a = 2$. Each face sheet of the shell has a thickness of $0.015 \times h_{total}$ and is made of composite material with the following properties: $E_1 = 172.5\,GPa$, $E_2 = E_3 = 6.9\,GPa$, $G_{12} = G_{13} = 3.45\,GPa$, $G_{23} = 2.76\,GPa$, $\nu_{12} = \nu_{13} = \nu_{23} = 0.25$. On the other hand, each core has a thickness of $0.4325 \times h_{total}$ and the material properties are the following: $E_1 = E_2 = 0.276\,GPa$, $E_3 = 3.45\,GPa$, $G_{12} = 0.1104\,GPa$, $G_{13} = G_{23} = 0.414\,GPa$, $\nu_{12} = 0.25$, $\nu_{13} = \nu_{23} = 0.02$. The total thickness is assumed to be $h_{total} = 1.0$. As in the previous analysis cases, the results are reported in non-dimensional form:

$$\hat{w} = \frac{10^2\, w\, E_{2_{(face\,sheets)}}\, h^3}{\hat{p}\, a^4} \qquad (\hat{\sigma}_{\alpha\alpha}, \hat{\sigma}_{\beta\beta}, \hat{\sigma}_{\alpha\beta}) = \frac{(\sigma_{\alpha\alpha}, \sigma_{\beta\beta}, \sigma_{\alpha\beta})\, h^2}{\hat{p}\, a^2} \qquad \hat{\sigma}_{\alpha z} = \frac{\sigma_{\alpha z}\, h}{\hat{p}\, a}$$

Different variable kinematic models have been used to perform the analyses of the shell structures. These models make use of various sublaminate groupings, which are summarized in the following by using the usual notation:

- $Case1 = \{layer1\}\,\{layer2, layer3, layer4, layer5, layer6, layer7, layer8, layer9, layer10\}\,\{layer11\}$
- $Case2 = \{layer1\}\,\{layer2\}\,\{layer3, layer4, layer5, layer6, layer7, layer8, layer9\}\,\{layer10\}\,\{layer11\}$
- $Case3 = \{layer1\}\,\{layer2\}\,\{layer3\}\,\{layer4, layer5, layer6, layer7, layer8\}\,\{layer9\}\,\{layer10\}\,\{layer11\}$
- $Case4 = \{layer1, layer2, layer3\}\,\{layer4, layer5, layer6, layer7, layer8\}\,\{layer9, layer10, layer11\}$
- $Case5 = \{layer1, layer2, layer3\}\,\{layer4\}\,\{layer5, layer6, layer7\}\,\{layer8\}\,\{layer9, layer10, layer11\}$
- $Case6 = \{layer1, layer2, layer3, layer4\}\,\{layer5, layer6, layer7\}\,\{layer8, layer9, layer10, layer11\}$
- $Case7 = \{layer1, layer2, layer3, layer4\}\,\{layer5\}\,\{layer6\}\,\{layer7\}\,\{layer8, layer9, layer10, layer11\}$

First a convergence study on the shell element was performed and it is shown in Table 11. For this analysis case, a composite sandwich cylindrical panel with circumferential length to thickness ratio $a/h = 5$ and side length ratio $b/a = 1$ is considered. Clearly, a mesh grid of 12×12 elements ensures the convergence in terms of both transverse displacement and the stresses. This mesh size is, thus, utilized for the remaining analyses.

Table 11: Convergence study. Composite sandwich cylindrical panel with circumferential length-to-thickness ratio $a/h = 5$ and side length ratio $b/a = 1$.

	Mesh	4×4	6×6	8×8	10×10	12×12	$ZIGT_a$[46]	$3D\ Elasticity$[47]
$LW4$	$\hat{w}\ (z = 0)$	5.2621	5.2593	5.2588	5.2587	5.2586	5.2616	5.2824
	$\hat{\sigma}_{\alpha\alpha}\ (z = -h/2)$	-2.1441	-2.0947	-2.0758	-2.0668	-2.0618	-2.1337	-2.0731
	$10 \times \hat{\sigma}_{\beta\beta}\ (z = +h/2)$	1.5573	1.5216	1.5086	1.5024	1.4990	1.4423	1.5395
	$\hat{\sigma}_{\alpha\beta}\ (z = -h/2)$	1.7780	1.6917	1.6603	1.6456	1.6375	1.6588	1.6409
	$\hat{\sigma}_{\alpha z}\ (z = 0)$	0.2140	0.2081	0.2061	0.2051	0.2046	0.2170	0.2001

The results from the variable kinematic models and from complete ESL and LW models are listed in Table 12 for various axis length-to-circumferential length ratios b/a and different circumferential length-to-thickness ratios a/h. In this table, the present CUF-based FEM results are compared with a 3D elasticity solution [47] and a layer-wise theory, called the zigzag theory (ZIGT). In particular, both analytical [46] and FEM [48] ZIGT solutions are given for comparison purposes. For the sake of completeness, the through-the-thickness behaviour of the stress components are also illustrated in Figs. 23 to 27. The behaviour of the variables along the thickness is invariant with respect to the b/a or a/h ratios. Thus, the case $b/a = 1$ and $a/h = 10$ is taken into account to plot the variables behaviour along the thickness in those figures. For the shell structures analysed in this section, the following considerations can be drawn:

- In terms of transverse displacement w, variable kinematic models with combined ESL/LW assumptions (i.e., $EL4_{,Case1}$, $EL4_{,Case2}$, $EL4_{,Case3}$, and $EL4_{,Case4}$) provide better accuracy with respect to the full ESL models, such as $EL4$, see Fig. 23. However, the best accuracy is reached assembling the sandwich cores with a layer-wise scheme while keeping the face composite sheets as ESL, i.e. $EL4_{,Case5}$. In this case, it is possible to reduce the computational costs in terms of degrees of fredoom as high as 53.33% with respect to a full LW reference solution. Variable kinematic models $EL4_{,Case6}$ and $EL4_{,Case7}$ still provide an improvement of the solution accuracy with respect to $EL4_{,Case1}$ to $EL4_{,Case4}$. Moreover, it is interesting to note that the $EL4_{,Case4}$ model has the same accuracy of the $EL4_{,Case3}$ model but with a DOFs reduction of 55.17%. Equivalently, $EL4_{,Case6}$ model has the same accuracy of the $EL4_{,Case7}$ model with a DOFs reduction of 38.09%.

- Figures 24 to 26 show that very small differences in terms of accuracy of $\sigma_{\alpha\alpha}$, $\sigma_{\beta\beta}$ and $\sigma_{\alpha\beta}$ distributions are visible in the composite sheets layers if $EL4_{,Case1}$ and $EL4_{,Case2}$ models are compared to $EL4_{,Case5}$, and $EL4_{,Case6}$ models. Nevertheless, $EL4_{,Case5}$, and $EL4_{,Case6}$ models provide the same solution of full refined LW model with a considerable reduction of the computational costs. For these stress components, the distribution within the core is roughly the same for all the models considered.

- As far as the shear stress $\sigma_{\alpha z}$ distribution is considered, Fig. 27 shows that all the variable-kinematic models provide results as accurate as the reference solutions in those layers that are approximated with a LW accuracy. This allows the analyst to choose the approximation accuracy in each thickness subdomain independently and save, eventually, computational costs but still having accurate solution in localized zones. For the analysis case under consideration, however, the best compromise between an accurate solution and an huge reduction of computational cost in terms of DOFs with respect to the full layer-wise solution, is obtained with the $EL4_{,Case5}$ model, whose DOFs reduction is 53.33%.

Table 12: Sandwich eleven-layered cylinder. Transverse displacement $\hat{w}(\alpha,\beta) = \hat{w}(a/2,b/2)$, in-plane stresses $\hat{\sigma}_{\alpha\alpha}(\alpha,\beta) = \hat{\sigma}_{\alpha\alpha}(a/2,b/2)$, $\hat{\sigma}_{\beta\beta}(\alpha,\beta) = \hat{\sigma}_{\beta\beta}(a/2,b/2)$, in-plane shear stress $\hat{\sigma}_{\alpha\beta}(\alpha,\beta) = \hat{\sigma}_{\alpha\beta}(0,0)$ and transverse shear stress $\hat{\sigma}_{\alpha z}(\alpha,\beta) = \hat{\sigma}_{\alpha z}(0,b/2)$.

		$a/h=5$					$a/h=10$					
	$z=$	$\hat{w}$ 0	$\hat{\sigma}_{\alpha\alpha}$ $-h/2$	$10\times\hat{\sigma}_{\beta\beta}$ $h/2$	$10\times\hat{\sigma}_{\alpha\beta}$ $-h/2$	$\hat{\sigma}_{\alpha z}$ 0	$\hat{w}$ 0	$\hat{\sigma}_{\alpha\alpha}$ $-h/2$	$10\times\hat{\sigma}_{\beta\beta}$ $h/2$	$10\times\hat{\sigma}_{\alpha\beta}$ $-h/2$	$\hat{\sigma}_{\alpha z}$ 0	$DOFs$
$b/a=1$	$3D\ Elasticity$[47]	5.2824	-2.0731	1.5395	1.6409	0.2001	2.5850	-1.9675	1.2612	1.4885	0.2021	
	$ZIGT_a$[46]	5.2616	-2.1337	1.4423	1.6588	0.2170	2.5762	-1.9776	1.2377	1.4893	0.2245	
	$ZIGT_{FE}$[48]	5.1264	-1.9903	1.4540	1.5745	0.2171	2.5024	-1.9228	1.2255	1.4369	0.2240	
	$LW4$	5.2824	-2.0848	1.5476	1.6595	0.2012	2.5850	-1.9786	1.2682	1.5055	0.2033	84375
	$LW1$	5.2775	-2.0858	1.5488	1.6588	0.2012	2.5847	-1.9790	1.2690	1.5053	0.2033	22500
	$EL3Z$	4.1624	-2.0624	1.5618	1.4801	1.2367	2.3091	-2.0089	1.3025	1.4260	1.2688	9375
	$EL4$	4.0764	-2.0717	1.4538	1.4712	0.9815	2.2918	-2.0163	1.2346	1.4239	1.0007	9375
	$EL1$	3.7660	-2.0435	1.4769	1.4030	0.6698	2.2028	-2.0122	1.3150	1.3891	0.6781	3750
	$EL4_{Case\,1}$	4.1405	-2.0819	1.4495	1.4870	0.9513	2.3072	-2.0153	1.2267	1.4295	0.9705	24375
	$EL4_{Case\,2}$	4.2709	-2.1075	1.4603	1.5093	0.9156	2.3379	-2.0199	1.2302	1.4384	0.9316	39375
	$EL4_{Case\,3}$	4.7676	-2.0863	1.5096	1.5837	0.7458	2.4609	-1.9976	1.2517	1.4728	0.7653	54375
	$EL4_{Case\,4}$	4.7675	-2.0865	1.5127	1.5837	0.7458	2.4609	-1.9977	1.2534	1.4728	0.7653	24375
	$EL4_{Case\,5}$	5.2822	-2.0850	1.5510	1.6595	0.1875	2.5849	-1.9786	1.2700	1.5054	0.1892	39375
	$EL4_{Case\,6}$	5.1562	-2.0918	1.5091	1.6422	0.1881	2.5525	-1.9821	1.2429	1.4962	0.1897	24375
	$EL4_{Case\,7}$	5.1564	-2.0918	1.5091	1.6423	0.2019	2.5525	-1.9821	1.2429	1.4962	0.2038	39375
$b/a=2$	$3D\ Elasticity$[47]	9.0416	-3.7989	1.3594	1.6680	0.3348	4.3974	-3.5216	0.9654	1.2841	0.3294	
	$ZIGT_a$[46]	9.0141	-3.9003	1.2524	1.6723	0.3650	4.3762	-3.5377	0.9380	1.2818	0.3667	
	$ZIGT_{FE}$[48]	8.6267	-3.5873	1.2445	1.5549	0.3585	4.1713	-3.3774	0.9154	1.2156	0.3590	
	$LW4$	9.0785	-3.8203	1.3665	1.6870	0.3367	4.3975	-3.5415	0.9707	1.2987	0.3313	84375
	$LW1$	9.0726	-3.8213	1.3658	1.6867	0.3368	4.3971	-3.5421	0.9706	1.2987	0.3313	22500
	$EL3Z$	7.1160	-3.7190	1.3297	1.4529	2.0518	3.8967	-3.5301	0.9950	1.2013	2.0438	9375
	$EL4$	6.9062	-3.6954	1.2053	1.4248	1.6129	3.8490	-3.5263	0.9191	1.1924	1.6043	9375
	$EL1$	6.3528	-3.6156	1.2343	1.3430	1.0941	3.6956	-3.5017	1.0058	1.1577	1.0835	3750
	$EL4_{Case\,1}$	7.0208	-3.7166	1.2043	1.4423	1.5647	3.8776	-3.5284	0.9102	1.1988	1.5572	24375
	$EL4_{Case\,2}$	7.2117	-3.7496	1.2193	1.4645	1.5003	3.9252	-3.5355	0.9157	1.2079	1.4938	39375
	$EL4_{Case\,3}$	8.1588	-3.7862	1.3000	1.5821	1.2388	4.1655	-3.5411	0.9450	1.2553	1.2380	54375
	$EL4_{Case\,4}$	8.1586	-3.7855	1.2983	1.5821	1.2388	4.1654	-3.5401	0.9408	1.2553	1.2380	24375
	$EL4_{Case\,5}$	9.0781	-3.8197	1.3652	1.6870	0.3139	4.3973	-3.5406	0.9667	1.2987	0.3085	39375
	$EL4_{Case\,6}$	8.8374	-3.8187	1.3192	1.6594	0.3140	4.3345	-3.5398	0.9465	1.2864	0.3086	24375
	$EL4_{Case\,7}$	8.8377	-3.8188	1.3193	1.6595	0.3369	4.3346	-3.5398	0.9465	1.2865	0.3314	39375

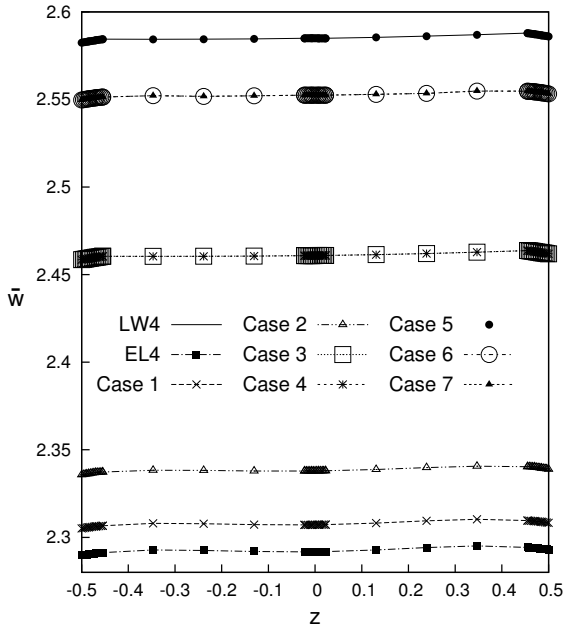

Figure 23: Sandwich eleven-layered cylinder. Transverse displacement w along the thickness, with axis length to circumferential length ratio $b/a = 1$ and circumferential length to thickness ratios $a/h = 10$.

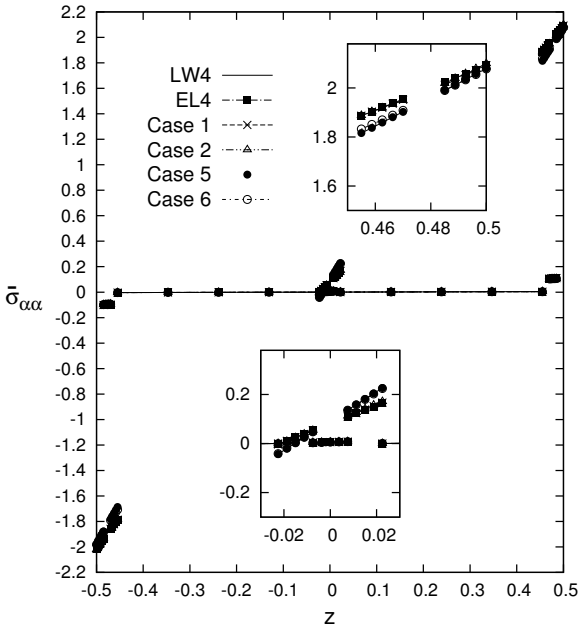

Figure 24: Sandwich eleven-layered cylinder. In-plane stress $\sigma_{\alpha\alpha}$ along the thickness, with axis length to circumferential length ratio $b/a = 1$ and circumferential length to thickness ratios $a/h = 10$.

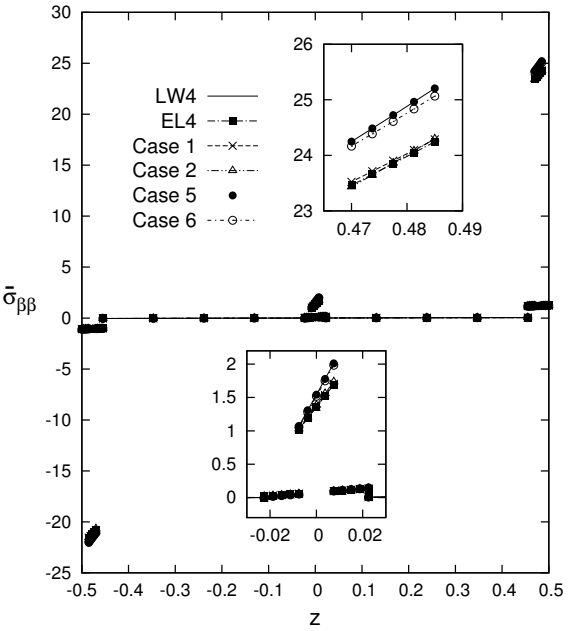

Figure 25: Sandwich eleven-layered cylinder. In-plane stress $\sigma_{\beta\beta}$ along the thickness, with axis length to circumferential length ratio $b/a = 1$ and circumferential length to thickness ratios $a/h = 10$.

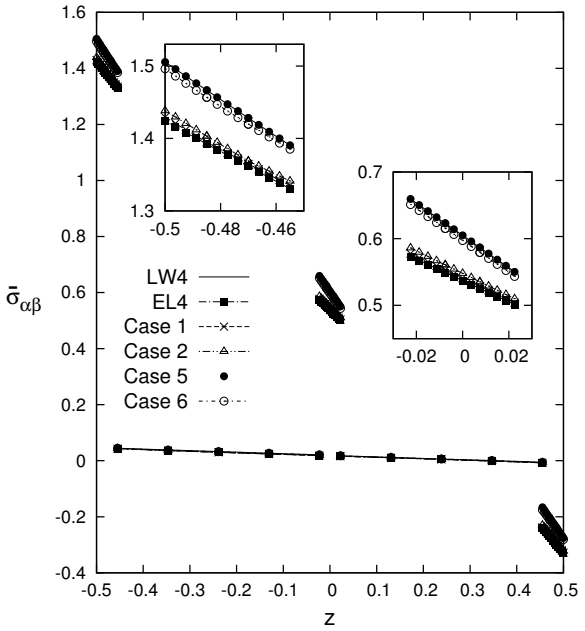

Figure 26: Sandwich eleven-layered cylinder. In-plane shear stress $\sigma_{\alpha\beta}$ along the thickness, with axis length to circumferential length ratio $b/a = 1$ and circumferential length to thickness ratios $a/h = 10$.

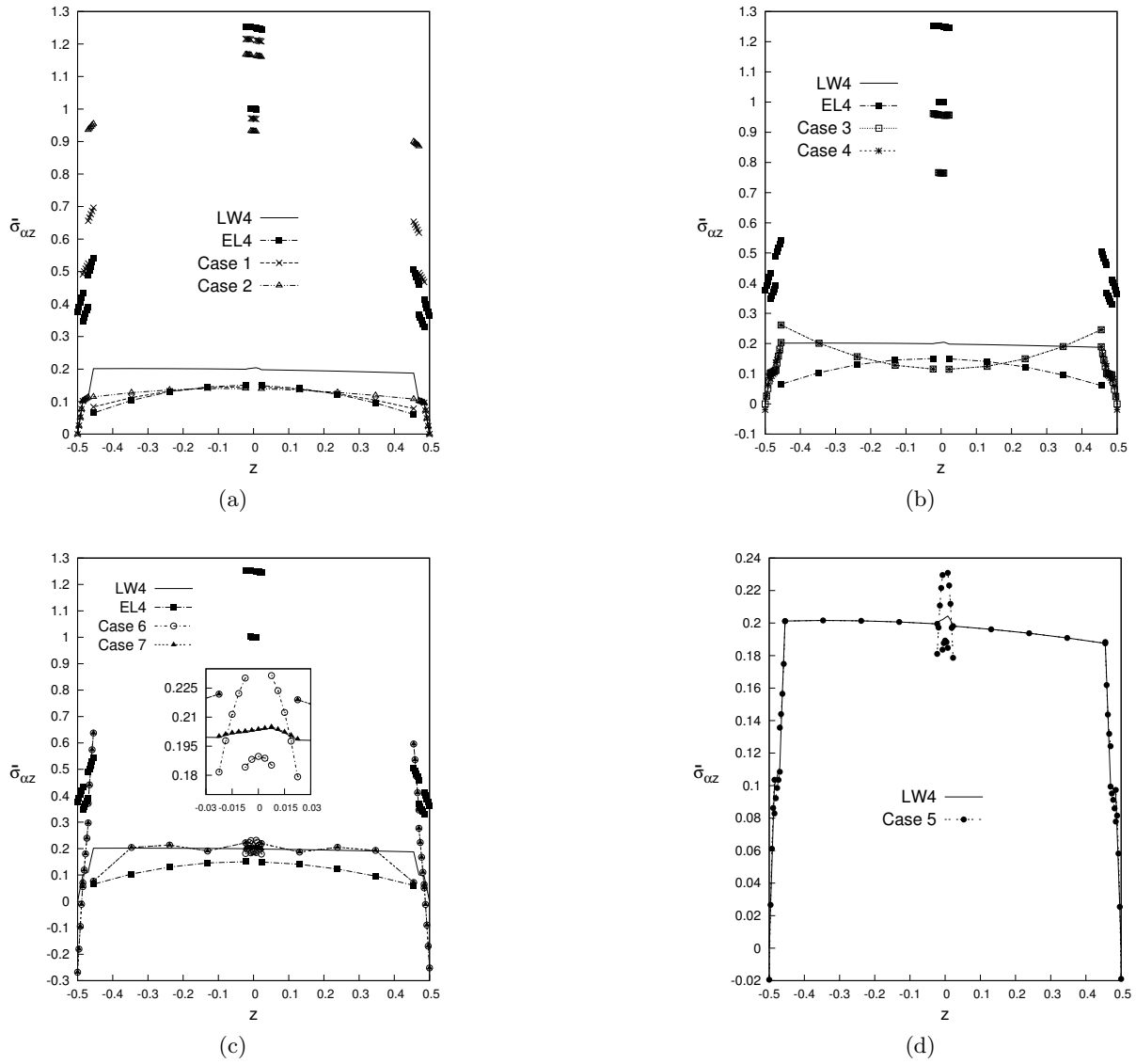

Figure 27: Sandwich eleven-layered cylinder. Transverse shear stress $\sigma_{\alpha z}$ along the thickness, with axis length to circumferential length ratio $b/a = 1$ and circumferential length to thickness ratios $a/h = 10$.

7 Conclusions

A new variable kinematic methodology for composite layered structures has been introduced in this paper. Based on the Carrera Unified Formulation (CUF), the proposed shell element employs displacement kinematics that can vary through the thickness of the structural domain. In this manner, low- to higher-order theories can be formulated straightforwardly and, thus, refined approximations and Layer-Wise (LW) descriptions of the mechanical unknowns can be utilized exclusively in those portions of the structure that requires a more detailed analysis. In fact, by using CUF and Legendre-like approximations of the shell displacement field, Equivalent-Single-Layer (ESL), LW and variable kinematic theories can be formulated arbitrarily and in a unified and hierarchical manner; the equilibrium equations and, eventually, the finite element arrays are written in terms of fundamental nuclei in the present formulation, and they can be arbitrarily expanded to any shell theory by using a recursive index notation.

The proposed model has been assessed through various numerical examples, including three and ten layered cross-ply shells subjected to bi-sinusoidal loads and simply-supported boundary conditions, mutilayered spherical panels under bi-sinusoidal loads, and sandwich cylinders undergoing a bi-sinusoidal pressure loadings. The results have been compared with those from the literature, already established CUF models, and elasticity solutions, whenever possible. The analysis of the results suggests the following conclusions:

- Because of its hierarchical capabilities, CUF is an effective tool for the implementation of variable kinematic shell theories.
- The proposed variable kinematic shell element allows to improve the solution locally and in a global/local sense. In other words, because it uses combined ESL and LW approaches within the same finite element, the accuracy of the shell model can be enhanced in those zones in the thickness domain where localized phenomena (e.g., concentrated stress/strain states, homogeneous boundary conditions, interlayer continuity, C_z^0 conditions, etc.) play a fundamental role.

References

[1] E Carrera. Historical review of Zig-Zag theories for multilayered plates and shells. *Applied Mechanics Review*, 56(3):287–308, 2003.

[2] J N Reddy and D H Robbins. Theories and computational models for composite laminates. *Applied Mechanics Review*, 47:147–165, 1994.

[3] T K Varadan and K Bhaskar. Review of different theories for the analysis of composites. *Journal of Aerospace Society of India*, 49:202–208, 1997.

[4] E Carrera. Developments, ideas and evaluation based upon Reissner's Mixed Variational Theorem in the Modeling of Multilayered Plates and Shells. *Applied Mechanics Review*, 54:301–329, 2001.

[5] W T Koiter. On the foundations of the linear theory of thin elastic shell. *Proc. Kon. Nederl. Akad. Wetensch.*, 73:169–195, 1970.

[6] P G Ciarlet and L Gratie. Another approach to linear shell theory and a new proof of Korn's inequality on a surface. *C. R. Acad. Sci. Paris*, I,340:471–478, 2005.

[7] C W Pryor and R M Barker. A finite element analysis including transverse shear effect for applications to laminated plates. *American Institute of Aeronautics and Astronautics Journal*, 9:912–917, 1971.

[8] A K Noor. Finite element analysis of anisotropic plates. *American Institute of Aeronautics and Astronautics Journal*, 11:289–307, 1972.

[9] T J R Hughes and T Tezduyar. Finite elements based upon Mindlin plate theory with particular reference to the four-node isoparametric element. *Journal of Applied Mechanics*, 48:587–596, 1981.

[10] T Kant, D R J Owen, and O C Zienkiewicz. Refined higher order Cˆ0 plate bending element. *Computer & Structures*, 15:177–183, 1982.

[11] T Kant and J R Kommineni. Large amplitude free vibration analysis of cross-ply composite and sandwich laminates with a refined theory and Cˆ0 finite elements. *Computer & Structures*, 50:123–134, 1989.

[12] J N Reddy. *Mechanics of Laminated Composite Plates and Shells: Theory and Analysis*. CRC Press, 1997.

[13] A N Palazotto and S T Dennis. Nonlinear analysis of shell structures. *AIAA Series*, 1992.

[14] H Murakami. Laminated composite plate theory with improved in-plane responses. *Journal of Applied Mechanics*, 53:661–666, 1986.

[15] U Iscsro. Eight node zig-zag element for deflection and analysis of plate with general lay up. *Composites Part B*, pages 425–441, 1998.

[16] V R Aitharaju and R C Averill. Cˆ0 zig-zag kinematic displacement models for the analysis of laminated composites. *Mechanics of Composite Materials and Structures*, 6:31–56, 1999.

[17] Y B Cho and R C Averill. First order zig-zag sublaminate plate theory and finite element model for laminated composite and sandwich panels. *Computer & Structures*, 50:1–15, 2000.

[18] A K Noor and W S Burton. Assessment of computational models for multi-layered composite shells. *Applied Mechanics Review*, 43:67–97, 1990.

[19] J N Reddy. An evaluation of equivalent-single-layer and layerwise theories of composite laminates. *Composite Structures*, 25:21–35, 1993.

[20] A S Mawenya and J D Davies. Finite element bending analysis of multilayer plates. *Journal for Numerical Methods in Engineering*, 8:215–225, 1974.

[21] F G Rammerstorfer, K Dorninger, and A Starlinger. Composite and sandwich shells. *Nonlinear Analysis of Shells by Finite Elements*, 328:131–194, 1992.

[22] A S D Wang and F W Crossman. Calculation of Edge Stresses in Multi-Layer by Sub-Structuring. *Journal of Composite Materials*, 12:76–83, 1978.

[23] N J Pagano and S R Soni. Global-Local Laminate Variational Model. *International Journal of Solids and Structures*, 19(3):207–228, 1983.

[24] R Jones, R Callinan, K K Teh, and K C Brown. Analysis of Multi-Layer Laminates Using Three-Dimensional Super Elements. *International Journal for Numerical Methods in Engineering*, 20(3):583–587, 1984.

[25] A Pagani, S Valvano, and E Carrera. Analysis of laminated composites and sandwich structures by variable-kinematic MITC9 plate elements. *Journal of Sandwich Structures and Materials*.

[26] M Botshekanan Dehkordi, M Cinefra, S M R Khalili, and E Carrera. Mixed LW/ESL models for the analysis of sandwich plates with composite faces. *Composite Structures*, 98:330–339, 2013.

[27] M Botshekanan Dehkordi, S M R Khalili, and E Carrera. Non-linear transient dynamic analysis of sandwich plate with composite face-sheets embedded with shape memory alloy wires and flexible core- Based on the mixed LW (Layer-wise)/ESL (Equivalent single layer) models. *Composites Part B*, 87:59–74, 2016.

[28] E Carrera. Theories and finite elements for multilayered, anisotropic, composite plates and shells. *Archives of Computational Methods in Engineering*, 9(2):87–140, 2002.

[29] E Carrera. Theories and finite elements for multilayered plates and shells: a unified compact formulation with numerical assessment and benchmarking. *Archives of Computational Methods in Engineering*, 10(3):215–296, 2003.

[30] K J Bathe and E Dvorkin. A formulation of general shell elements - the use of mixed interpolation of tensorial components. *International Journal for Numerical Methods in Engineering*, 22:697–722, 1986.

[31] K J Bathe, P S Lee, and J F Hiller. Towards improving the MITC9 shell element. *Computers and Structures*, 81:477–489, 2003.

[32] K J Bathe and F Brezzi. A simplified analysis of two plate bending elements-the MITC4 and MITC9 elements. *Proceedings, Numerical Methods in Engineering: Theory and Applications*, 1987.

[33] N C Huang. Membrane locking and assumed strain shell elements. *Computers and Structures*, 27(5):671–677, 1987.

[34] E Carrera. An assessment of mixed and classical theories for the thermal stress analysis of orthotropic multilayered plates. *Journal of Thermal Stresses*, 23(9):797–831, 2000.

[35] M Cinefra, S Valvano, and E Carrera. Heat conduction and Thermal Stress Analysis of laminated composites by a variable kinematic MITC9 shell element. *Curved and Layered Structures*, 1:301–320, 2015.

[36] M Cinefra, E Carrera, and S Valvano. Variable Kinematic Shell Elements for the Analysis of Electro-Mechanical Problems. *Mechanics of Advanced Materials and Structures*, 22(1-2):77–106, 2015.

[37] M Cinefra, S Valvano, and E Carrera. A layer-wise MITC9 finite element for the free-vibration analysis of plates with piezo-patches. *International Journal of Smart and Nano Materials*, 6(2):85–104, 2015.

[38] E Carrera. Multilayered shell theories accounting for layerwise mixed description, Part 1: governing equations. *AIAA Journal*, 37(9):1107–1116, 1999.

[39] E Carrera. Multilayered shell theories accounting for layerwise mixed description, Part 2: numerical evaluations. *AIAA Journal*, 37(9):1117–1124, 1999.

[40] T J R Hughes, M Cohen, and M Horaun. Reduced and selective integration techniques in the finite element methods. *Nuclear Engineering and Design*, 46:203–222, 1978.

[41] M. Cinefra and S. Valvano. A variable kinematic doubly-curved MITC9 shell element for the analysis of laminated composites. *Mechanics of Advanced Materials and Structures*, 23(11):1312–1325, 2016.

[42] E. Carrera, M. Cinefra, M. Petrolo, and E. Zappino. *Finite Element Analysis of Structures through Unified Formulation*. John Wiley & Sons, Chichester, West Sussex, UK., 2014.

[43] T.K. Varadan and K. Bhaskar. Bending of Laminated Orthotropic Cylindrical Shells - An Elasticity Approach. *Composite Structures*, 17:141–156, 1991.

[44] J.N. Reddy and C.F. Liu. A higher-order shear deformation theory of laminated elastic shells. *International Journal of Engineering Science*, 23(3):319–330, 1985.

[45] A. Kumar, A. Chakrabarti, and M. Ketkar. Analysis of laminated composite skew shells using higher order shear deformation theory. *Latin American Journal of Solids and Structures*, 10:891–919, 2013.

[46] P.C. Dumir, J.K. Nath, P. Kumari, and S. Kapuria. Improved efficient zigzag and third order theories for circular cylindrical shells under thermal load. *Journal of Thermal Stresses*, 31:343–363, 2008.

[47] S. Kapuria, P.C. Dumir, and S. Sengupta. Nonaxisymmetric exact piezothermoelastic solutions for laminated cylindrical shell. *AIAA Journal*, 35:1792–1795, 1997.

[48] Y.M. Yasin and S. Kapuria. An efficient layerwise finite element for shallow composite and sandwich shells. *Composite Structures*, 98:202–214, 2013.